Autonomous Cooperative Routing for Mission-Critical Applications

Ahmed Bader and Mohamed-Slim Alouini

Abstract We are entering an era where three previously decoupled domains of technology are rapidly converging together: robotics and wireless communications. We have seen giant leaps and improvements in computational efficiency of vision processing and sensing circuitry coupled with continuously miniaturized form factors. As a result, a new wave of mission-critical systems has been unleashed in fields like emergency response, public safety, law enforcement, search and rescue, as well as industrial asset mapping. There is growing evidence showing that the efficacy of team-based mission-critical systems is substantially improved when situational awareness data, such as real-time video, is disseminated within the network. Field commanders or operation managers can make great use of live vision feeds to make educated decisions in the face of unfolding circumstances or events. In the likely absence of adequate cellular service, this translates into the need for a mobile ad hoc networking technology (MANET) that supports high throughput but more importantly low end-to-end latency. However, classical MANET technologies fall short in terms of scalability, bandwidth, and latency; all three metrics being quite essential for mission-critical applications. The real bottleneck has always been in how fast packets can be routed through the network. To that end, autonomous cooperative routing (ACR) has gained traction as the most viable MANET routing proposition. Compared to classical MANET routing schemes, ACR is poised to offer up to 2X better throughput, more than 4X reduction in end-to-end latency, while observing a given target of transport rate normalized to energy consumption. Nonetheless, ACR is also associated with a few practical implementation challenges. If these go unaddressed, it will deem ACR practically infeasible. In this chapter, efficient and low-complexity remedies to those issues are presented, analyzed, and validated. The

A. Bader · M.-S. Alouini (✉)
Computer, Electrical, and Mathematical Science and Engineering (CEMSE) Division,
King Abdullah University of Science and Technology (KAUST),
Thuwal, Makkah Province, Saudi Arabia
e-mail: slim.alouini@kaust.edu.sa

H. M. Ammari (ed.), *Mission-Oriented Sensor Networks and Systems: Art and Science*, Studies in Systems, Decision and Control 164,
https://doi.org/10.1007/978-3-319-92384-0_2

validation is based on field experiments carried out using software-defined radio (SDR) platforms. This chapter sheds light on the underlying networking challenges and practical remedies for ACR to fulfill its promise.

Keywords Autonomous cooperative routing
Mobile ad hoc networks (MANET) · Mission-critical applications
Situational awareness · Real-time video streaming · Path-oriented routing
Geographical routing · End-to-end latency · Normalized transport rate
Cooperative transmission · Carrier frequency offset (CFO)
Software-defined radio (SDR)

1 Introduction

1.1 Team-Based Mission-Critical Applications

Broadly speaking, mission-critical applications are defined as those applications demanding data delivery bounds in the time and reliability domains [1]. When a critical mission is executed by a cluster or swarm of a human and/or robotic agents it is typically referred to as a team-based mission-critical operation [2]. In the abstract sense of things, a mission-critical agent is only able to execute its mission when equipped with the right sensory and possibly actuation gear. Thus, mission-oriented wireless sensor networks (the core subject of this book) and team-based mission-critical operations clearly intersect.

Recently, there has been an unprecedented growth in the use of computer vision in mission-critical applications [3]. The dissemination of live vision-based data feeds offers great visibility into the underlying process being monitored, mapped, or controlled [4, 5]. Live video streaming is believed to offer significant improvement in the decision-making abilities in the face of unexpected events [6]. As a matter of fact, the use of real-time video and vision-based data streaming for enhancing the contextual awareness levels has been lately earning substantial interest in other relevant domains such as telemedicine [7], paramedics [8], emergency and first response [9], law enforcement, and tactical (military) operations [10].

The availability of live video feeds is crucial in boosting situational and contextual awareness. It is argued that human decision-making failures during time- and mission-critical scenarios can be caused by shortage of understanding of the underlying situation and inability to understand the context [6]. Field commanders are consistently required to take decisions in response to events occurring in the field. There is appreciable evidence that acquiring access to live video feeds streamed from front-end personnel diminishes uncertainty and therefore upgrades the decision-making quality [9, 11]. It is not only raw-format video that proves to be useful, but other formats can even have more utility such as thermal vision data during hydrocarbon leak detection for instance.

The virtue of real-time vision-based data sharing in boosting the operational efficiency of mission-critical operations is hopefully quite intuitive. Human agents can make better decisions when offered timely information and deeper visibility into the ongoing physical process being treated [12]. Research has also shown that the availability of real-time video communications for paramedics and emergency responders significantly enhances collaborative execution of a mission and reduces time to completion [11]. Therefore, we have seen more emphasis on real-time video streaming for mission-critical operations in literature. For example, the U.S. National Institute of Standards and Technology (NIST) has lately released a technical note [13] in which the significance of real-time streaming for public safety operations is clearly underscored.

Real-time streaming from the field can be well extended to additional use cases in other industrial verticals. Two general categories of mission-critical applications are addressed herewith:

(1) Defense and emergency response operations mainly encompassing tactical missions, law enforcement, firefighting, search and rescue, crowd management, and telemedicine.
(2) Industrial field operations mainly in hydrocarbon exploration and production (E&P), mining, and power generation. Within this context, it is often required to dispatch crews of technicians and engineers to the field to execute a certain time-critical maintenance routine, react to a process failure, or treat a chemical spill.

In both categories, front-end field personnel are equipped with sensory that feeds back critical information to the back-end decision-making central. Such information is analyzed manually and/or automatically before commands and actuation instructions are fed forward to the front-end.

An example of a public safety mission-critical operation is illustrated in Fig. 1. From a networking viewpoint, data flow in mission-critical applications is mainly dictated by the underlying decision-making mechanism. Teams deployed into the field typically follow a hierarchical command chain [6]. Attempting to process or even just view the data by front-end personnel may cause distraction. Hence, decision-making by far is largely concentrated at the back-end point. This implies that the network has to generally operated according to a "convergecast" rather than peer-to-peer mode.

Figure 1 also showcases a growing trend toward future mission-critical MANET. It is envisioned that unmanned autonomous vehicles (UAV) will be deployed as front-end agents [2]. Here, swarms of aerial or terrestrial UAVs are dispatched into the field to execute a mission under human supervision and control. In mission-critical applications, a paramount task is the joint planning and optimization of motion trajectories of the human and robotic agents [14]. The timeliness of disseminating path planning and control signaling messages is quite instrumental [2]. This places

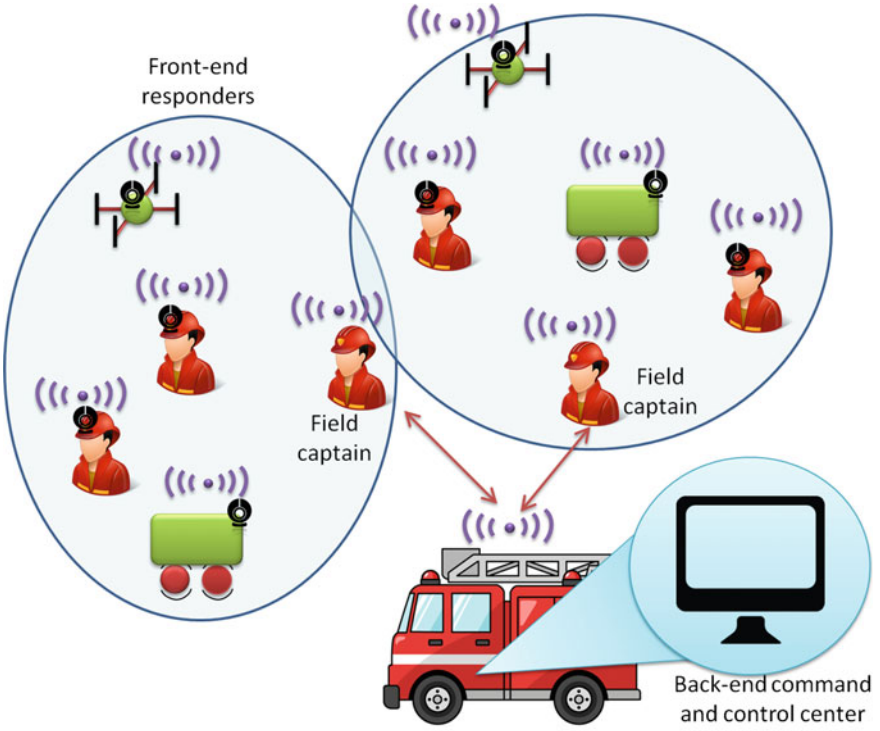

Fig. 1 An example of public safety MANET use case. Situational awareness data (video, thermal imaging, pressure, and temperature readings) flows toward the field commander and eventually to the back-end command and control center. Commands and actuation instructions are fed forward to front-end personnel as well as unmanned autonomous vehicles (UAV). Actuation instructions may include opening/closing a gate, controlling a valve, spraying of chemicals, etc.

yet an additional level of significance for designing low-latency MANET routing schemes.

The introduction of UAVs is also expected to go mainstream in mission-critical industrial operations. One example is the use of UAV swarms for thermal imaging and remote sensing [15]. UAVs can be deployed in industrial facilities as a routine maintenance measure, or as part of an emergency response operation. It is also noteworthy to mention at this point that UAV swarms have been also considered for 3D mapping, surveying, and other civil engineering tasks [16]. Again, the value proposition of deploying UAVs alongside human agents is manifested in the reduction of time to complete a mission, reduce injury rates, achieve better field coverage, and improving accessibility into hard-to-reach spots.

2 Mobile Ad Hoc Routing Revisited

By nature, real-time video streaming applications are typically delay-intolerant. Needless to say that vision-based data is also bandwidth-hungry. From a wireless networking perspective, it is indeed always desirable to capitalize to the maximum extent possible on the economies of scale offered by off-the-shelf standardized technologies. Hence, the natural technology candidates are LTE and Wi-Fi. Nonetheless, there are unfortunately some inherent deficiencies in LTE and Wi-Fi systems which render them less attractive, particularly for applications of mission-critical nature.

LTE as a cellular technology is ubiquitous but only to a limited extent. It is straightforward to argue that there will be situations and circumstances where adequate LTE service is not available [17]. Examples include remote onshore industrialized sites, offshore oil rigs, or deep mining pits. In fact, even in urbanized areas where coverage *does* exist, field personnel may have to be deployed in hard-to-reach areas where LTE does not penetrate indoors deeply enough.

Another interesting example where LTE is highly likely to fall short is massively crowded events [18]. In such contexts, the sheer scale of the load that LTE networks have to withstand has an adverse effect on the bandwidth and delay performance for mission-critical applications. One may argue that mission-critical applications are typically granted preemption on the radio access network (RAN) interface by mobile operators [19]. This is a valid argument so long as the mission-critical user equipment (UE) has already managed to gain access to the network. However, gaining access to the RAN in the first place may suffer from tremendous latencies and escalated rates of failure [20]. This specifically true under high user/traffic intensities; something which is quite expected in massively crowded events. The same rationale also applies during times of natural disasters when attempts to place calls on the network throttles the network.

Unlike LTE, Wi-Fi is more of a portable technology. This is actually meant in the sense that Wi-Fi hotspots[1] can be deployed by field personnel right in the area where action is taking place. However, due to regulatory and inherent design constraints, Wi-Fi only offers a limited reach when deployed as a single-hop network.

Attempts to extend Wi-Fi service coverage span can be accomplished by means of multihop networking. However, real-world deployments have repeatedly reported some hard limits on the number of hops that Wi-Fi-based solutions can sustain [21]. This is in part due to the excessive medium access control (MAC) layer overhead plaguing Wi-Fi. As a matter of fact, the IEEE 802.11ax standard (expected to be released in 2019) is already working on means to streamline the MAC and reducing the mean time to accessing the medium [22].

Having said that, the underlying MAC layer in Wi-Fi is not fully to blame. A major contributor to the non-scalability of Wi-Fi in multihop contexts is the routing overhead. This has been coined by some researchers as a cause of "capacity deficit" [23] and recognized as a major challenge by the Defense Advanced Research Projects

[1] LTE-Unlicensed hotspots is obviously a very comparable option to Wi-Fi. In other words, it will suffer more or less from the same scalability issues outlined herewith for the case of Wi-Fi.

Agency (DARPA) [24]. Such a deficit or shortcoming tends to have a more profound effect as the scale (number of users and/or traffic intensity) increases as well as with increased mobility.

As a result, there is an obvious need for infrastructure-independent ad hoc networking with strong support for mobility. Clearly, this can be articulated as a quest for a high-throughput low-latency mobile ad hoc network (MANET). Consequently, proprietary tailor-made MANET technologies are resurfacing again as viable propositions for mission-critical operations [25].

Undoubtedly, multihop MANET research literature has a mature legacy of work that is at least a couple of decades old. However, the need for significantly more bandwidth per user, ultralow end-to-end (e2e) latency, and tangibly better scalability calls for going back to the drawing board [26]. This is true since classical routing schemes are plagued by protocol overheads which have the tendency to substantially throttle the end-to-end performance of the MANET [27, 28].

To alleviate the routing overhead problem, autonomous cooperative routing (ACR) comes to rescue. In ACR, routing decisions are taking locally, i.e., wireless nodes do not revert to cross-coordination between each other before a packet is forwarded [29]. In fact, ACR does not revert to the classical concept of point-to-point (PTP) routing [26]. Rather than searching for the optimal path in a graph-based representation of the network, ACR features a seamless flow of the packet from source to destination based on a many-to-many communications paradigm [30, 31]. Any node receiving a packet will inspect its attributes based on which it decides whether to forward the packet or not. As such, the terms "routing" and "relaying" are used interchangeably throughout this chapter.

The MANET application scenarios considered herewith feature traffic flows which are predominantly convergecast. In other words, packets are unicast in the upstream direction to a single sink. To that end, current ACR schemes are not *fully* autonomous when it comes to unicast traffic. This is true since an end-to-end handshake must take place between each traffic source and the network sink. Such a handshake is necessary to define a "barrage" region (also referred to as a "suppression" region) between each source–sink pair. The said region serves to confine the traffic flow within certain geographical boundaries [28].

The handshake process required for spatial containment of traffic flows has to be revisited whenever significant topological changes occur, e.g., due to mobility [28]. To circumvent such a shortcoming, a novel method for constructing a fully autonomous cooperative routing (FACR) scheme is presented in this chapter. The method relies on the use of a novel physical layer (PHY) frame structure coupled with geographical (position-based) routing criteria.

Recognizing the advantages of ACR/FACR in addressing mission-critical application needs, this chapter unveils a few design challenges associated with these systems. The chapter mainly focuses on those prime challenges which are essential for any practical and technically feasible implementation of ACR/FACR. Practical hardware and software solutions to those challenges are presented and discussed in depth. The practicality of the proposed solutions is validated on software-defined radio (SDR) platforms.

The developed hardware and software is used to carry out field tests for the sake of empirical assessment of the performance, primarily the PHY layer. The end goal is to not only to offer a public-domain insight into how ACR/FACR can be practically implemented, but also on the outstanding throughput and latency performance of this class of MANET routing.

3 Autonomous Cooperative Networking Solutions

This section mainly aims to lay down the foundation for the subsequent discussion on the virtues of autonomous cooperative networking, and in particular how routing takes place. An analytical overview is provided with regard to why this relatively new class of MANET technologies not only challenges a stagnant MANET R&D ecosystem but also is better positioned to meet the aspirations of team-based mission-critical systems.

3.1 Autonomous Cooperative Routing Background

The goal of this subsection is not to offer a detailed literature survey of ACR-driven routing schemes. Rather, it aims at offering a brief historical background and some insight into the motivations for ACR. In the next subsections, some of the most prominent incentives for adopting ACR schemes are presented in more depth.

The field of mobile ad hoc networking (MANET) is a long-established field with a broad coverage in research literature. One of the most important topics addressed in MANET research is routing. For a long period of time, point-to-point (PTP) routing schemes (also known as path-oriented schemes [32]) were prevailing in literature as well as practical implementations [26]. Within this realm, geographical routing (geo-routing) has been widely accepted for routing in MANETs. This is mainly due to its resilience to mobility and network topological changes [33]. In fact, geo-routing was adopted by the European Telecommunications Standards Institute (ETSI) as a standard MANET routing scheme for Intelligent Transport Systems (ITS) [34].

Notwithstanding early signs of success, current implementations of geo-routing are highly likely to be plagued by an overhead that grows rapidly with node density and/or frame arrival rate [29]. This indeed has a negative impact on latency and throughput. Such an issue has already been identified as a priority to be addressed for scalable MANETs [23, 24].

Generally speaking, classical geo-routing schemes belong to one of two groups. The first is beacon-based whereby position beacons are exchanged between neighboring nodes, so as to maintain up-to-date topological awareness. On the other hand, beaconless geo-routing entails receiver-based contention to select the best packet forwarder [31]. Nonetheless, both forms suffer from the aforementioned problem: they are highly inclined to produce large overheads. This is either due to the repetitive

exchange of neighbor discovery messages (true for beacon-based protocols) or due to contention resolution overhead (applies to the beaconless case) [35].

Needles to reiterate that the routing protocol overhead must be decreased in order to meet the aspirations set forth for mission-critical applications. To serve exactly that purpose, cooperative transmission comes to rescue. From a conceptual point of view, autonomous cooperative relaying was first introduced in [36, 37]. The forwarding mechanism there was labeled as "randomized distributed cooperative transmission". Autonomous cooperative transmission was analyzed from the perspective of achievable cooperative transmit diversity in great depth in [38, 39].

In essence, autonomous cooperative relaying entails the forwarding of physical frames while not reverting to any relay selection process. The term *autonomous* mainly stems from the fact that nodes within a cooperative cluster are actually unaware of each other [26]. In other words, there does not exist any sort of cross-coordination between nodes before the frame is relayed. Therefore, autonomous cooperative routing is also often referred to as "blind cooperative transmission" [40].

The transformation of ACR concepts into practice entailed the need to find means for confining the packet flows spatially. Otherwise, unicast flows will quickly flood the network and unnecessarily hijack the spatial and temporal resources of the network [31]. As such, controlled barrage or suppression regions must be created by means of request-to-send (RTS)/clear-to-send (CTS) handshake between any arbitrary pair of source–sink nodes [26]. Traffic from a source to a given sink is suppressed and barred to spill outside the designated barrage region [30]. This line of work has been holistically treated in a series of chapters in [10, 25, 26, 28, 41]. To guarantee positive progress toward the sink, hop count to reach the sink is adopted as a routing metric.

In case position information is available to nodes, then position-based routing criteria can be used to streamline the forwarding process within narrow geographical corridors [29]. One possible manifestation of such approach is illustrated in Fig. 2. As shown in the figure, only nodes offering positive progress toward the sink take on the responsibility of forwarding the packet. Once a node receives a packet, it inspects the position attributes of the transmitters and compares them to its own. The PHY header has to be designed in a way that supports such a functionality as further described in Sect. 4.2. A simple geo-routing criterion is to for the receiver to forward the packet if it is closer than at least a certain number of transmitters.

The concurrent transmission of the same PHY frame provides for an array gain that is proportional to the number of transmitters at a given hop [30]. Such a gain contributes to the increase in the average hop distance and consequently reduces the e2e latency. Nonetheless, it also means substantially higher energy consumption per frame at a single hop. This important trade-off is analyzed and treated rigorously from an e2e perspective in [29]. It is shown there that for a given e2e energy consumption target, ACR can be tweaked to offer tangibly lower e2e latency.

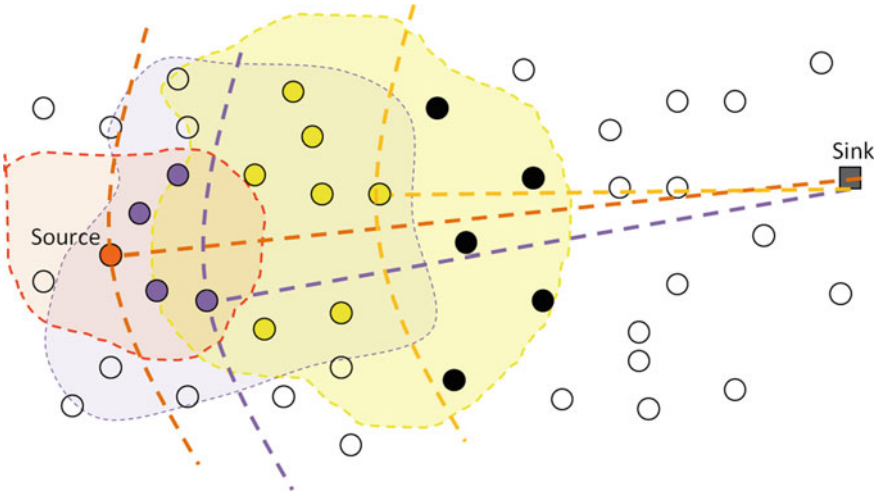

Fig. 2 Illustration of the operation of an autonomous cooperative scheme. A source injects a frame into the network. Receivers who are closer to the sink than the source will relay the frame. In the second hop, each receiver reads the position information conveyed by the transmitters of the first hop in order to decide whether to forward the frame or not. Any second-hop receiver offering positive progress toward the sink will forward it. The forwarding process continues seamlessly until the frame reaches its destination

3.2 Why Autonomous Cooperative Routing?

In this section, the advantages of ACR in comparison to path-oriented (i.e., PTP-based) routing schemes are studied. Three prime metrics are considered herewith: end-to-end latency, normalized transport rate, and maximum achievable throughput. A list of all notations used in the chapter is given in Table 1.

3.2.1 Lower End-to-End Latency

The end-to-end latency is given by $\sum_{q=1}^{Q} T_{h_q}$. Here, Q denotes the expected number of hops from source to sink assuming that a barrage (i.e., suppression) region has already been allocated for a given traffic flow. Further, T_{h_q} is the duration of the qth hop. In the case of ACR, the hop duration T_{h_q} is deterministic since there is no contention among potential relays. Accordingly, $T_{h_q} = T_p + T_t$, where T_p is the packet duration and T_t is the turnaround time corresponding to the change from receiver state to transmitter state.

On the other hand, path-oriented routing schemes entail some overhead pertaining to the selection of the optimal path. In the sequel, classical beaconless geo-routing is considered as a representative example. The sender needs to select the best relay, typically the one offering largest positive progress toward the destination. The selection

Table 1 List of notations

T_p	Data packet duration	T_t	Time to transition between Tx and Rx states
T_c	Control packet duration	T_w	Waiting time before successful channel access
T_b	Fixed back-off timer	T_{h_q}	Duration of the qth hop
Q	Average number of hops to destination	d	Hop distance
T_R	PHY header duration	P_t	Transmit power
P_n	Noise power	τ	Threshold on outage probability
γ_t	SINR for successfully decoding a frame	α	Large-scale path loss coefficient
γ_o	Mean SINR	a	Hop distance gain of ACR over PTP
I	Number of cooperative transmitters	N	Number of nodes in the network
$p(N)$	Probability that a node is a destination	$A(N)$	Area of the communications footprint
R_{max}	Maximum achievable per-node throughput	W	Over-the-air bit rate
P_b	Back-off probability	D	Source–destination separation
l_A	Packet arrival rate	l_e	Effective packet arrival rate in case of path-oriented routing
λ	Wavelength		
ρ	Node density	$\overline{M}$	Average number of nodes backing off
Δ_f	Subcarrier bandwidth	N_s	FFT size
$T_s = \frac{1}{N_s \Delta_f}$	Sampling time	$t = nT_s$	Discrete time representation
$k = -\frac{N}{2} \cdots \frac{N}{2}$	Subcarrier index	$i = 1 \ldots I$	Coop.transmitters
δ_i	CFO of ith Tx with respect to Rx	$a_{k,n} e^{j\phi_{k,n}}$	QAM symbol time n and subcarrier k
$h_{i,m}, m = 1 \ldots \mathcal{M}$	Channel fading coefficients	T	Time between multipath channel components
$T_i^{'}$	Propagation delay plus cooperative time offset associated with transmitter i	T_s	Signal sampling interval
		x_i^n	Phase rotation of the ith coop.transmitter
$N^{'}$	Number of nodes (barrage region update)	T_U	Total duration to update barrage regions
S_R	Number of times barrage update is repeated	$\mathcal{C}(\mathcal{UV})$	Number of hops measured from node $\mathcal{U}$ to V
B_L	Number of localization resource blocks	B_q	Number of relative position quantization tones
p_{st}	Probability of successful triangulation	F	Number of trials before successful triangulation
L	Number of bits in a data packet	P_o	Outage probability

is established through a handshake process. At the bare minimum, such a process consists of three transactions at *each* hop [35]:

(1) Request-to-send (RTS) message of duration T_c followed by a turnaround time T_t.
(2) A clear-to-send (CTS) message from the optimal receiver with duration that is also equal to T_c followed by T_t.
(3) Packet transmission with duration T_p.

The hop duration is therefore $T_{h_q} \geq T_p + 2T_t + 2T_c$ which is obviously always greater than that of the autonomous case. Therefore, end-to-end latency as a performance metric speaks in favor of ACR.

There is another factor that further boosts the latency performance of ACR. That is related to the fact that ACR exploits cooperative transmission techniques which in return feature array (power) gains [30]. Moreover, with some precoding and transmit-side signal processing, transmit diversity gains can be also attained [38]. By means of applying carefully selected randomization matrices to the transmitter vectors, such diversity gains can be obtained. To some extent, this approach has similar effect to the so-called phase dithering [42].

The array and diversity gains result in extending the average communication range compared to path-oriented routing. Undoubtedly, this results in reducing the number of hops Q, thus further contributing to the reduction of the end-to-end latency [43]. This is true since $\sum_{q=1}^{Q} T_{h_q}$ is a decreasing monotone in Q. A rigorous analysis of the progress made per hop in ACR networks can be found in [29].

3.2.2 Higher Normalized Per-Hop Transport Rate

The normalized transport rate (NTR) is defined as the average number of bits that can be communicated at a given hop over distance per unit time using one unit of energy [44]. The consideration of the normalized transport rate as a performance metrics stems from its ability to capture hop distance (which eventually affects end-to-end delay) as well as energy consumption.

Recalling that a contention phase ought to take place before a packet is routed in path-oriented schemes, then the upper bound on NTR is dictated by two factors:

(1) The minimum duration of a contention phase.
(2) The maximum achievable hop distance.

The hop distance has many definitions in literature, but here it is assumed that it refers to the positive progress made at a given hop along the line connecting the source to the destination. In the case of path-oriented schemes, assuming the mean hop distance to be equal over all hops is an acceptable approximation (especially in dense scenarios) [32, 45].

The hop distance, denoted by d, is governed by the underlying outage model. In a Rayleigh fading channel, the mean signal-to-noise and interference ratio (SINR) is given by

$$\gamma_o = \frac{2P_t}{P_n}\left(\frac{\lambda}{4\pi d}\right)^{\alpha}, \tag{1}$$

where λ is the wavelength, α is the large-scale path loss coefficient, P_t is the transmit power, and P_n is the noise power. The outage probability is given by $\mathrm{P}_o = 1 - e^{-\gamma_t/\gamma_o}$, where γ_t is the below which the receiver will be in outage. Consequently, the hop distance given a single transmitter d is expressed as

$$d \leq \left(\frac{\lambda}{4\pi}\right)\sqrt[\alpha]{\frac{2P_t \ln\frac{1}{1-\tau}}{P_n\gamma_t}}. \tag{2}$$

On the other hand, the duration of one complete contention phase cannot be shorter than one RTS message from the sender, one CTS message from the relay, plus the packet duration, T_p. As mentioned earlier, the half-duplex nature of the devices entails a turnaround time of T_t. Accordingly, the NTR for PTP-based routing is upper bounded by

$$NTR_{PTP} = \frac{Ld}{\left[2(T_c + T_t) + T_p\right]P_t(T_p + 2T_c)}, \tag{3}$$

where L is the length of a packet in bits. On the flip side of the coin, the NTR for the autonomous case is given by

$$NTR_{ACR} = \frac{Lda}{(T_p + T_R)^2 IP_t}, \tag{4}$$

where I is the number of cooperative transmitters, T_R is the duration of the PHY header, and a is a gain factor which reflects the fact that the hop distance in cooperative transmission mode is generally larger than PTP mode. There are indeed many factors affecting the value of a. Nonetheless, for the sake of simplification and conciseness of the analysis, the special case of I equidistant transmitters can be considered here. In such a case, $a = I^{1/\alpha}$. Accordingly, it can be shown from (3) and (4) that ACR-based systems offer better NTR under the condition that

$$I^{1-\frac{1}{\alpha}} < \frac{[2(T_c + T_t) + T_p](T_p + 2T_c)}{(T_p + T_R)^2}. \tag{5}$$

The values of T_p, T_c, T_t and T_R are mainly dictated by the underlying video transmission quality of service (QoS) requirements as well as hardware constraints.

In Sect. 6, a proprietary PHY implementation developed for this project is described in more detail. The implemented PHY is based on the use of orthogonal frequency division multiplexing (OFDM). The duration of one OFDM symbol is set at 8 μs. The duration of the PHY header is equal to 1 OFDM symbol. The preamble training sequence has the duration of exactly 38.4 μs. Therefore, the

shortest frame (i.e., one that is sufficiently large to carry an RTS or CTS control message) is $T_c = 54.4\,\mu s$. The turnaround time, T_t, is highly dependent upon the underlying radio front-end. In this specific implementation, it was measured to be around 180 μs.[2] Finally, the payload portion was set to consist of 50 symbols. While lower frames may be preferable from a frame error rate (FER) viewpoint, they are associated with larger PHY overhead ratio. A frame of 50 symbols, i.e., $T_p = 476.8\,\mu s$, strikes the right balance.

Based on the above, and assuming a path loss coefficient of $\alpha = 3$, then ACR outperforms PTP-based path-oriented scheme for $I < 3.02$. In other words, autonomous geo-routing offers higher NTR as long as is carried out by one, two, or three transmitters at a given hop.

3.2.3 Higher Maximum Achievable Throughput

The end-to-end latency performance is indicative but not sufficient to establish with evidence the superiority of ACR. Interference caused by other concurrent packet flows indeed has an adverse effect on e2e latency since it causes transmission outages and invokes back-off procedures. Hence, it must be taken into consideration. The interplay between interference and medium access is best captured by studying the maximum achievable throughput per node.

It was shown in [32] that ACR-based networks offer a per-node unicast capacity which scales in the order of $\Theta(\sqrt{N/\log N})$. This is identical to the Gupta–Kumar per-user capacity [46] that traditional path-oriented routing networks can offer. While such a result is reassuring, asymptotic scaling orders do not suffice to benchmark ACR against path-oriented PTP-based routing schemes. Furthermore, video streaming traffic in a mission-critical MANET is predominantly convergecast. As such, this must be taken into consideration.

Bisnik and Abouzeid provided a detailed throughput and delay analysis in a random access multihop network [47, 48]. For a network of N nodes, an absorption probability $p(N)$ is defined therewith as the probability that a traffic flow is terminated at an arbitrarily chosen node. It is straightforward to state that $p(N) = 1/N$ in a convergecast network.

Assuming a persistent back-off scheme [49], the mean waiting time before successful channel access is denoted by T_w. The back-off footprint, $A(N)$ is defined as the area around a given transmitter within which no other transmission can take place due to interference. $A(N)$ is actually normalized by the total area of the network. Finally, the maximum achievable throughput per node, R_{max}, is defined to be the maximum node throughput for which the end-to-end delay remains finite. Subsequently, R_{max} (in bps) is computed using [47], Eq. (22):

[2] A video capture of the turnaround time measurement is posted online for the interested reader (https://youtu.be/lDYVHZ6GcIM).

$$R_{max}(N) = \frac{Lp(N)}{T_w + \frac{L}{W} + 4NA(N)\frac{L}{W}}, \\ = \frac{L}{NT_w + NT_h + 4N^2A(N)T_h}, \tag{6}$$

where W is the bit rate.

The mean waiting time T_w is function of the back-off probability. The latter can be expressed as $P_b = \overline{M}/N$, where $\overline{M}$ is the average number of nodes that are forced to queue at least one frame of their own during the entire multihop journey of another frame [50]. Assuming Bernoulli distribution, the mean number of transmission attempts before success is $1/P_b$. As such, the mean back-off time can then be expressed as

$$T_w = (1 - P_b)T_b = \left(\frac{N}{N - \overline{M}}\right) T_b, \tag{7}$$

where $T_b \geq T_h$ is a fixed duration a node must wait before reattempting to retransmit.

To compute $\overline{M}$, first the probability that exactly m nodes will back off during a given hop is analyzed. Given n nodes exist in the back-off region and a packet arrival rate of l_A, then this probability is given by

$$p_m(m|n) = \binom{n}{m} \left(1 - e^{-T_h l_A}\right)^m \left(e^{-T_h l_A}\right)^{n-m}, m \leq n. \tag{8}$$

The probability that exactly n nodes actually exist in the region is

$$p_n(n) = \frac{1}{n!}(\rho A)^n e^{-\rho A}, \tag{9}$$

where ρ is the network node density under the assumption of 2D Poisson point process node distribution. Consequently, the probability distribution function of m is given by

$$p_m(m) = \sum_{n=m}^{\infty} p_m(m|n)p_n(n). \tag{10}$$

The next question to tackle: in light of the above, what is the probability, $P_M(M)$, that M sensor nodes backlog at least one transmission during the Q-hop lifetime of the packet in concern? The different permutations for distributing those M nodes over Q hops can be conveniently computed using integer set partitioning algorithms. These permutations can be expressed in matrix format as

$$\begin{bmatrix} m(1,1) & \dots & m(1,Q) \\ \vdots & \ddots & \vdots \\ m(\mathcal{P},1) & \dots & m(\mathcal{P},Q) \end{bmatrix} \in \mathbb{Z}^{\mathcal{P}\times Q}, \tag{11}$$

where $\mathcal{P}$ equals the number of different permutations corresponding to the distribution of M back-off nodes over Q hops. Consequently, the probability density function is obtained as follows:

$$P_M(M) = \sum_{u=1}^{\mathcal{P}} \prod_{i=1}^{Q} p_m(m(u,i)). \tag{12}$$

Therefore, a compact expression for $\overline{M}$ can be obtained as follows:

$$\overline{M} = \sum_{M=0}^{\infty} \sum_{u=1}^{\mathcal{P}} \prod_{q=1}^{Q} \sum_{n=m(u,q)}^{\infty} M p_m(m|n) p_n(n). \tag{13}$$

Substituting (13) into (7) gives the mean waiting time before successful channel access, T_w. It is paramount however to note that listen-before-talk (and consequently back-off procedures) is applied only once at the source in case of autonomous routing. On the other hand, it is applied at *each* intermediate hop in case of PTP-based (i.e., path-oriented) routing. In other words, the back-off procedures are invoked every time a node has a packet to send whether its own or an ingress packet from a neighboring node. Hence, the effective packet arrival rate in case of path-oriented routing is actually

$$l_e = \frac{l_A}{p(N)} = N l_A. \tag{14}$$

The computation of T_w and subsequently R_{max} is highly dependent on the mean number of hops, Q, as can be inferred from the analysis above. For a source–destination separation of D, the average number of hops in PTP-based systems is more or less $Q = \lceil D\sqrt{\frac{\pi}{A(N)}} \rceil$. On the other hand, such an approximation does not hold true in ACR-based systems. This is because in the long-term average sense, the hop distance grows in size every hop [29, 30]. As such, it is mandatory to derive a means to compute the probability mass function (PMF) of Q, which is the task to tackle next.

The probability of hopping Q times before reaching the destination is expressed as $p_Q(Q) = \mathbb{P}[x_Q \geq D]$, where x_Q is the total progress made after Q hops along the axis connecting the source and the destination. The number of cooperative transmitters at hop i is denoted by I_i. Further, the cumulative number of cooperative transmitters from the first hop till the $(Q-1)$th hop is given by $S_{Q-1} = \sum_{i=1}^{Q-1} I_i$.

An expression for the total progress made by the packet after Q hops was derived in Eq. (9) of [29] and is recalled here for convenience:

$$x_Q = \varphi S_{Q-1} + (Q-1)\frac{\beta}{U^{\frac{1}{\alpha}}} + x_1. \tag{15}$$

In (15), φ and β are network-dependent parameters, α is the large-scale path loss exponent, x_1 is the progress made in the first hop, and U is and outage-dependent constant that is given by [29]:

$$U = \frac{P_n}{2P_t}\left(\frac{4\pi}{\lambda}\right)^{\alpha}\frac{\gamma_t}{\ln\frac{1}{1-\tau}}. \tag{16}$$

It was also demonstrated in [29] that the PMF of S_{Q-1} can be computed for a given set of network parameters by recursion. Therefore, the PMF $p_Q(Q)$ can be computed numerically using

$$p_Q(Q) = \mathbb{P}\left[S_{Q-1} \geq \frac{1}{\varphi}\left(D - \frac{\beta}{U^{1/\alpha}}(Q-1) - x_1\right)\right]. \tag{17}$$

With the PMF readily available, the mean value of Q can be then easily computed.

The ratio of R_{max} for ACR to that of PTP-based was computed using (6)–(17). Results are shown in Fig. 3 in terms of the communication range gain, a. For a better and more insightful perspective, the e2e latency reduction factor that ACR enjoys over PTP-based routing is also plotted on the same figure. The plot in Fig. 3 is divided into 3 segments corresponding to the number of cooperative transmitters covering a given range of gain. Empirical results obtained from field testing and reported in Sect. 5 have been used to deduce the value of I (the number of cooperative transmitters) corresponding to a range of values for a (the ACR hop distance gain).

Although a larger gain favors ACR in terms of end-to-end latency, it is not always preferable in terms of throughput performance. It is evident from the figure that ACR starts to lose its edge in terms of per-node throughput as the gain increases. This is mainly because the coverage footprint of a packet transmission grows, thus blocking other nodes from accessing the network [32]. As such, it is essential to tune down the individual transmit power so that the gain is maintained within limits.

3.2.4 Summary

It is worthwhile at this point to summarize the key findings so far. To compare ACR to classical path-oriented routing schemes, it is best to fix the NTR as a performance constraint since it is the one that captures energy consumption. It has been already shown that with $I = 3$, ACR and path-oriented schemes offer the same NTR. However, it is clear from Fig. 3 that ACR offers up to 2X improvement in the maximum achievable throughput per node. It can be also inferred that ACR enjoys at least 4X reduction in the end-to-end latency. A corollary to this statement is that if throughput and latency targets are fixed, ACR will consume substantially less energy per transported bit. Looking at it from either perspective, ACR outperforms classical PTP-based path-orient MANET routing by far.

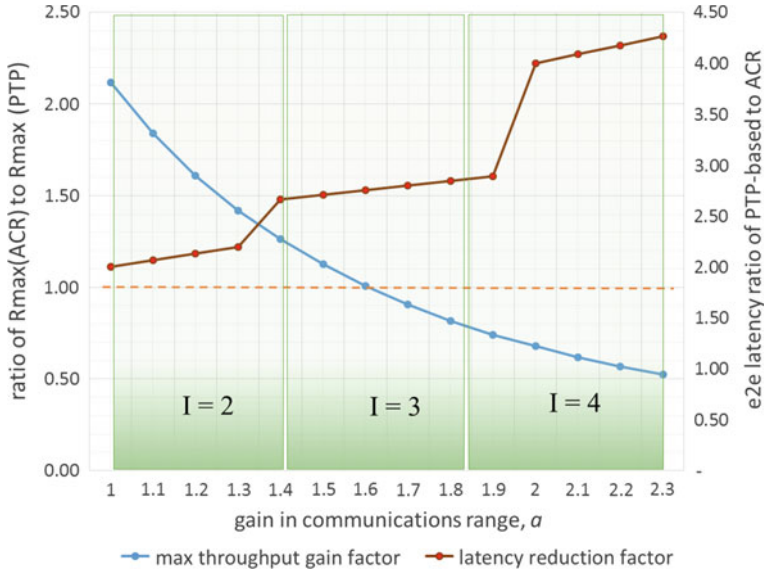

Fig. 3 The performance of ACR is compared to PTP-based routing in terms of maximum achievable per-node throughput as well as end-to-end latency. Using the analytical results of Sect. 3.2, the computations were carried out assuming a network of 20 nodes at a density of $\rho = \frac{1}{30^2}\text{m}^{-2}$. The average PTP communication range was $\leq$20 m at a path loss coefficient of 2.8. Packet duration of 0.5 ms is assumed at an arrival rate of 100 s^{-1}

A final note should be tailored for security aspects. Indeed, security is a paramount concern in mission-critical applications and should not be overlooked. However, it is quite an involved task to benchmark the performance of ACR protocols to path-oriented ones in terms of susceptibility to malicious attacks. Recognizing its importance, analysis of security aspects for ACR is left as future scope of work.

4 A Higher Degree of Autonomy

While autonomous cooperative routing (ACR) has been shown to offer an undeniable value proposition, there is more that can be achieved within its realm. In this section, we describe the motivation for developing a *fully* autonomous cooperative routing technique. We also highlight some of the key design elements as well as practical implementation considerations.

4.1 Motivation

Route stability is defined as the probability that an end-to-end path connecting source to destination is still available after a certain duration from being established [51]. Indeed, ACR has been shown to offer better route stability compared to path-oriented MANET routing schemes under realistic mobility models [28]. In other words, ACR-based MANETs are substantially more tolerant to topological changes. Nevertheless, barrage regions still need to be maintained and regularly updated.

A barrage region must be initially created then regularly updated for each source–destination pair. In a convergecast mode (which is typical in mission-critical applications), this mandates the execution of a round-trip end-to-end handshake between each node in the network and the network sink. For a given node $\mathcal{U}$, the handshake process between $\mathcal{U}$ and the sink is essentially designed so that all other nodes can measure how many hops away from $\mathcal{U}$ they are [25]. This is then used to carve the barrage region from $\mathcal{U}$ to the sink. Denoting the hop count from $\mathcal{U}$ to another node $\mathcal{V}$ with $\mathcal{C}(\mathcal{U}\mathcal{V})$, then a simple rule is to have nodes with $\mathcal{C}(\mathcal{U}\mathcal{V}) > Q(\mathcal{U})$ suppress the transmission of $\mathcal{U}$'s packets [26].

While traffic in convergecast networks is predominantly upstream (traffic toward the sink), there is the need to cater for downstream traffic encompassing control and configuration messages. It is inaccurate however to consider that the barrage region in the upstream direction is good enough to represent that in the reverse direction, i.e., downstream. Reciprocity on weighted graphs (such as wireless networks) is a highly contentious issue [52]. As such, routes are generally nonreciprocal, and consequently, a barrage region has to be separately created for each direction of the traffic.

There are surely multiple approaches to manage the barrage region update process. It is important to note that the network can handle only one handshake process at a time. This is true since messages emanate from or terminate at a single node. Therefore, it is quite challenging to handle more than one update process at a time due to interference constraints. In other words, the network sink is required to orchestrate the barrage region update process. Assuming the sink has prior knowledge of all mobile nodes in the network, then one feasible approach consists of three phases:

(1) A broadcast message from the sink soliciting a response from node $\mathcal{U}$. Intermediate nodes relaying the response message increment a designated hop count field in the packet as it traverses the network toward $\mathcal{U}$.
(2) A response message which is broadcast from node $\mathcal{U}$ back to the sink. Any intermediate node relaying the response message performs two tasks:
    (a) Increments a designated hop count field in the packet as it traverses the network toward the sink.
    (b) Takes a decision whether it lies within or outside the downstream barrage region of $\mathcal{U}$.

(3) To shape the upstream barrage region of $\mathcal{U}$, the sink has to rebroadcast another message containing the hop count $Q(\mathcal{U})$ measured on the previous message. As this message traverses the network, each intermediate relay node decides whether it belongs within or beyond the upstream barrage region.

The process above is then sequentially repeated across the whole node population. Putting things into perspective, as the number of nodes N gets larger, the barrage region update process starts to have a tangibly significant overhead. This issue is discussed next.

In mission-critical operations, it is reasonable to mandate that all of the nodes complete the barrage creation/update process. Otherwise, nodes which are left out (for one reason or another) will resort to broadcasting, i.e., flooding, all of their frames. Undoubtedly, this causes substantial interference and unnecessarily overgrazes the network's spatial and temporal resources. As such, the barrage region creation/update process should target a 100% reachability. Reachability is a metric that measures the percentage of nodes which can be covered, i.e., are reachable, after performing $\mathcal{X}$ broadcast rounds [53]. Reachability is denoted by a positive monotonic function $R(\mathcal{X}) \leq 1$, where $\mathcal{X} = 0 \ldots \mathcal{X}_{max}$, $R(\mathcal{X}_{max}) = 1$, and $R(0) = 0$.

The barrage region handshake process has to be effectively executed with each node as many times as needed to reach that node. This actually contributes to increasing the duration of the barrage creation/update process. Subsequently, the effective number of nodes can be essentially defined as the number of times the handshake process is executed until barrage regions for all nodes have been established. Taking into consideration the fact that the handshake process consists of three broadcast phases, then the effective number of nodes is therefore given by

$$N^{'} = N \left(\sum_{\mathcal{X}=1}^{\mathcal{X}_{max}} \mathcal{X} \left[R(\mathcal{X}) - R(\mathcal{X}-1) \right] \right)^{3}. \tag{18}$$

Another major factor to be considered relates to the fact that the hop count is not a deterministic parameter but rather a discrete random variable. This is a fact of crucial importance since the hop count from the source to the sink as well as to the intermediate nodes is the sole parameter used in defining the barrage region [26]. The number of hops measured from the traffic source $\mathcal{U}$ to an intermediate relay node $\mathcal{V}$ at around $\mathcal{X}$ is denoted by $\mathcal{C}_{\mathcal{X}}(\mathcal{UV})$. As a matter of fact, (17) can be used to derive the PMF of $\mathcal{C}(\mathcal{U})$ by substituting Q with $\mathcal{C}_{\mathcal{X}}(\mathcal{UV})$ and making D equal to the distance between the $\mathcal{U}$ and $\mathcal{V}$.

Denoting the average hop count by $\overline{\mathcal{C}}(\mathcal{UV})$, it can be demonstrated numerically that the probability $\mathbb{P}[\mathcal{C}_{\mathcal{X}}(\mathcal{UV}) \neq \overline{\mathcal{C}}(\mathcal{UV}]$ has an appreciable value. An immediate conclusion can be drawn: the three-way handshake process must be carried out more than once for each node, i.e., $S_R \geq 2$ times, in order to come up with an acceptable estimate of $\mathcal{C}(\mathcal{UV})$. Analysis of S_R and its relation to the confidence intervals of $\mathcal{C}(\mathcal{UV})$ is actually left off as follow-up work to this chapter.

Based on all of the above, the total time required to finish the barrage region creation/update process is given by

$$T_U = 3Q_{max}N^{'}T_hS_R, \tag{19}$$

where Q_{max} is the maximum number of hops required for the broadcast message to reach all nodes in the network. It is insightful at this point to put things into perspective using a numerical example. In [28] (Fig. 4), it was shown that path availability probability drops below 95% after approximately 25–50 s.[3] Tactical and mission-critical MANETs can typically have as many 100 nodes [26]. Nodes are spread out such that up to 10 hops may be needed for a broadcast message to cover the network [28]. The hop duration can be assumed to be in the range of $T_h = 500\,\mu$s which includes a very short packet transmission time, processing time, and radio turnaround time. The effective number of nodes is highly influenced by $R(1)$ which is typically in the range of 95% [53]. Taking $R(\mathcal{X}) = [0.950, 0.990, 0.999, 1.000]$, then $N^{'} = 119$. Assuming $S_R = 2$, then (19) yields a whopping $T_U = 3.57$ s! This is at 14–28% contribution to the protocol overhead.

The barrage region creation/update overhead should also account for cases of network entry, i.e., new nodes joining the network. Join events will cut off the live network operation for a non-negligible period of time. So based on all of the above, there is sufficient rationale and motivation to fortify ACR with *full* autonomy, the subject of which is discussed in the next section.

4.2 Full Autonomy Enabled by Geo-routing

What would it take for a node to locally decide whether it should forward a given source's packet or not? What if a node is equipped with the capability to qualify whether its participation in the forwarding process is beneficiary to the packet's progress toward the sink? The availability of such a capability unleashes fully autonomous cooperative routing.

Knowledge of position relative to the sink is sufficient to meet that goal. During network initialization phase, the source sends a broadcast packet informing all other nodes of its position. Each node is also required to acquire its position relative to the sink. This can be done by means of an onboard global positioning system (GPS) module. Contrary to the classical perception, low-power GPS modules have been commercially available for quite some time. As a matter of fact, power consumption by the GPS module is far less significant than other key components in wireless

[3]The choice of a value for the path availability metric is indeed relative and subject to the underlying application. In mission-critical applications, robustness and high reliability are often stressed as key performance indicators by end users. Thus, selecting 95% as a benchmark mainly stems from feedback the authors accumulated through interactions with end users.

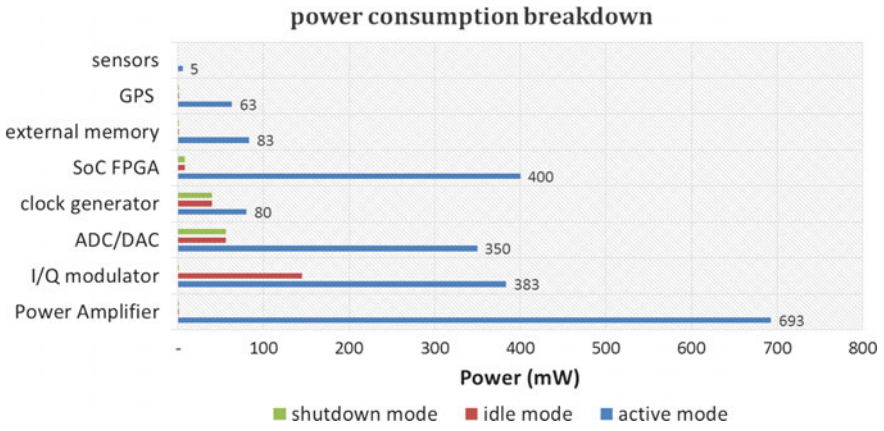

Fig. 4 Various candidates for each component in the system have been surveyed by the authors with low power consumption as a prime objective. The survey quickly revealed that the analog front-end components (i.e., I/Q, PA, ADC/DAC) are the most power-hungry. Duty-cycling these components whenever possible is not only a good practice but a necessity. The power budget of the GPS module can be considered as insignificant

communications systems. For instance, the analog front-end is far more power-hungry than the GPS module as illustrated in Fig. 4. Furthermore, the GPS module can be deeply duty-cycled to further save power.

The availability of position information allows the coupling of geo-routing and autonomous cooperative transmission. The result is full autonomy. This has been already eluded to in the illustration offered in Fig. 2 in Sect. 3.1. Full-length GPS positions are not really needed. Instead, each node needs to compute its relative position vector (distance and azimuth) with the origin being the sink. Furthermore, the system design has to cater for the very likely situation of weakening or complete blackout of the GPS signal.

Fortunately, the timescale of node mobility is quite relaxed: losing the GPS signal for a few seconds is likely to induce only intangible changes in the network topology. So it is more of an opportunistic approach which is advocated herewith where the position vector is updated whenever the GPS signal is accessible. Nonetheless, to account for those cases where a subset of nodes may suffer from prolonged GPS signal loss, a cooperative localization method is presented later in this section.

From a practical point of view, the challenge concerns the means by which cooperative transmitters can convey their position information to receivers (i.e., nodes which are the potential next-hop forwarders). An inherently related challenge is for this means to concurrently support the self-localization capability. The solution addressing both requirements is presented in the next subsection.

4.3 Random Access

To facilitate the communication of position information by transmitters, random access resources are allocated within the PHY frame [54] as shown in Fig. 5. The random access (RA) area consists of two distinct parts. The first one contains a total of B_Q tones which are allocated for progress quantization purposes. The second part is consists of B_L resource blocks distributed over b OFDM symbols and are allocated explicitly for localization purposes. The design and processing considerations of the localization part of the RA area is discussed in the next subsection.

Before a cooperative transmitter sends a frame, it quantizes the progress it offers with respect toward the sink. There are B_Q quantization levels such that resolution is D/B_Q, where D is the distance between the source and the sink. Each step is allocated exactly one tone in the random access area shown in Fig. 5. The relay needs to indicate the quantized progress it offers by simply energizing the corresponding tone whose index is equal to its progress level. Simple on-off keying (OOK) binary modulation is used to modulate the respective tone. At the receiver side, the B_Q tones will be routed from the output of the FFT stage toward the OOK demodulator as shown in Fig. 6. Progress levels of the respective transmitters are extracted and fed to a routing decision module.

Again, it is worthwhile to put things into perspective from a practical point of view. Nodes can be assumed to be distributed over a finite 2D disk with diameter D_{max} according to a binomial point process (BPP) [55]. However, in a geo-routing context, the progress along the line connecting source to destination is what really matters. As such, the 2D BPP distribution can be projected or more precisely reduced to a 1D

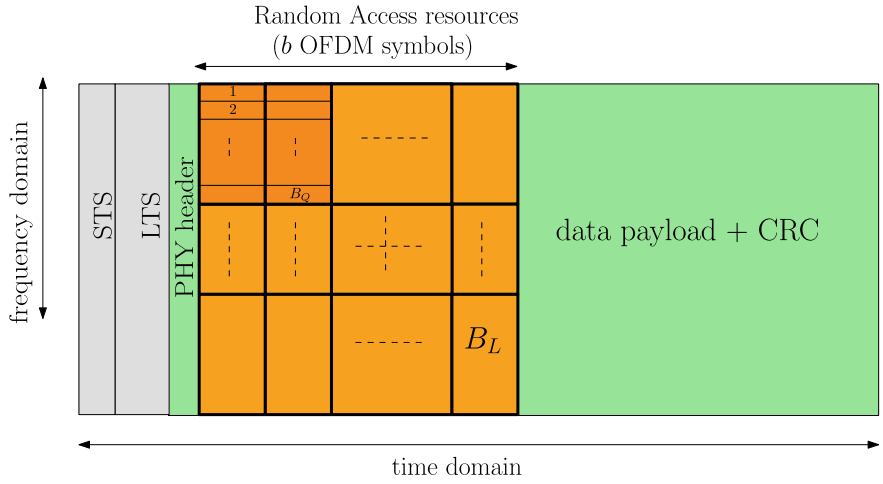

Fig. 5 A random access (RA) area is inserted into the OFDM frame to support two capabilities: (1) allow cooperative transmitters to indicate the progress they offer toward the sink, and (2) encode their position information that can be used by receiver so as to perform a TDOA-based self-localization

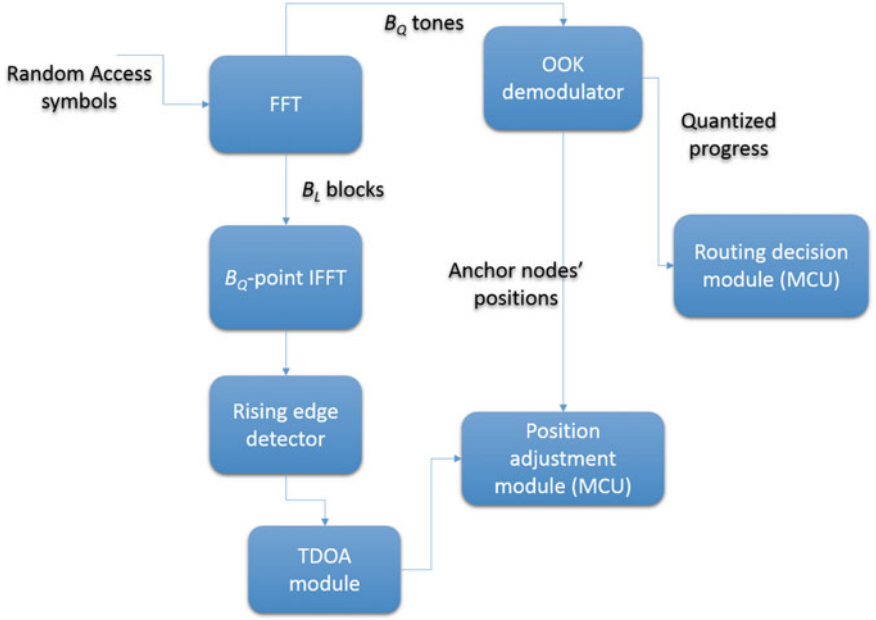

Fig. 6 A block diagram illustrating the processing of the quantization tones and localization resource blocks, both part of the random access area illustrated in Fig. 5

distribution. Consequently, the average distance to the ith nearest neighbor along the 1D progress dimension is given by $\frac{1}{2}ID_{max}/(N+1)$ [55]. The progress quantization level must be made sufficiently small to accommodate node displacement patterns. One viable design criterion is to have the quantization step D_{max}/B_Q larger than the distance to the Ith nearest cooperative transmitter along the progress line. In other words, it is to have

$$B_Q \geq 2(N+1)/I. \tag{20}$$

For $N = 100$ and $I = 3$ nodes, then $B_Q \geq 68$ tones which can be easily allocated within the stretch of one or two OFDM symbols.

4.4 Self-localization Scheme

It has already been shown by [28] that it takes 25–50 s before the end-to-end path starts to become obsolete under realistic mobility models. A corollary to this is that nodes can afford to lose their GPS signals for an equivalently long duration. Nonetheless, there might be situations where some nodes may suffer from GPS signal blackouts for even longer durations. Mission-critical systems have to incorporate higher levels

of resilience and robustness by definition and therefore need to account for such corner cases.

Nodes can capitalize on the presence of the random access area to carry out a triangulation procedure [54]. Those nodes which enjoy clear GPS signals can transmit their position information on regular basis so that others without GPS access localize themselves. As shown in Fig. 5, the random access area incorporates B_L resource blocks just for that purpose.

The method proposed for self-localization is to compute time difference of arrival (TDOA) [54]. Therefore, localization resource blocks need to cater two pieces of information: position information of the transmitters and propagation delay differences. The first one is straightforward and entails each anchor node encoding its position information into one of the localization blocks. A block is selected randomly by an anchor node and therefore collisions may occur. This is further discussed at the end of this subsection. Within this context, anchor nodes simply represent that subset of transmitter nodes which still enjoy clear access to the GPS signal.

On the other hand, extraction of TDOA information exploits the fact that each uniquely selected resource block contains a signal with a unique time signature. This is further illustrated in Fig. 7. The time reference at the receiver is influenced by the first energy arrival in the preamble portion of the frame. The B_L time waveforms must be reconstructed in order to detect the offset of each one from the zero time reference. As such, the B_L blocks are fed sequentially back to a B_Q-point IFFT module as depicted in Fig. 6. The TDOA can then be measured.

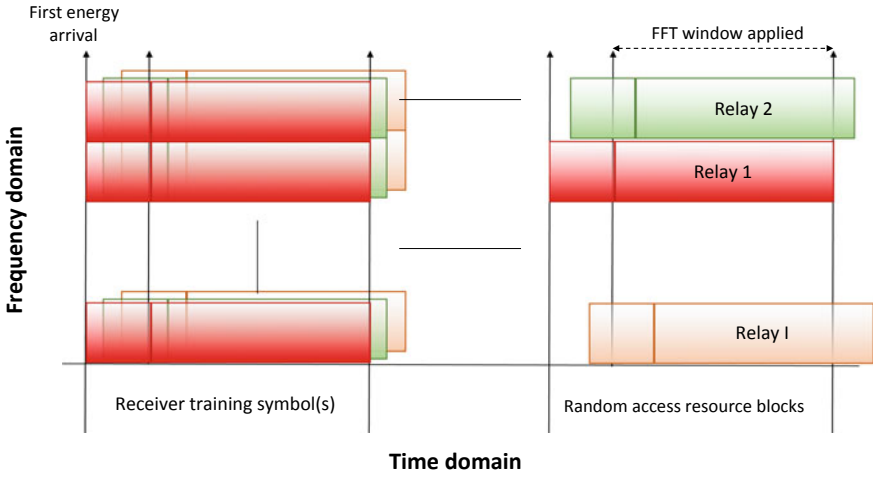

Fig. 7 The localization random access resource blocks are offset from each other in time. This is due to the fact that each block is modulated by a different transmitter (obviously as long as it happens to be selected by one transmitter)

Inherent to any random access methodology, collisions may occur. Therefore, a sufficient number of resource blocks B_L should be allocated. It has been shown in [29] that when I nodes randomly access B_L random access resource blocks, the probability of at least $z \leq B_L$ uniquely selected blocks can be evaluated recursively using

$$p_z = p_{z-1} \left(\frac{B - z}{B - z + 1} \right)^{I-z}, \tag{21}$$

where $p_o = 1$. For triangulation purposes, at least three nodes are required. Subsequently, the success probability of self-localization for given received frame is given by

$$p_{st} = \prod_{z=1}^{3} \left(\frac{B_L - z}{B_L - z + 1} \right)^{I-z}, B_L \geq 3. \tag{22}$$

The number of frames until the triangulation function succeeds is denoted by F. Had I been constant, the mean F would have been represented by a geometric random variable whose mean is $\mathbb{E}[F] = 1/p_{st}$. Nonetheless, I is also randomly distributed and understanding its statistical behavior is nothing but trivial. This is true especially since the value of I depends on a multitude of factors including packet forwarding statistics and GPS signal loss patterns.

Having said that, I is expected to grow whenever the receiver is closer to the network sink and/or the GPS signal is less likely to be blocked. If I tends to be large, $\mathbb{E}[F]$ will also be, i.e., it will take a few frames before a node with lost GPS signal can triangulate itself. Fortunately, however, when I tends to be large, this also implies that the expected number of nodes with lost GPS signal is small.

In any case, one can obtain a practical flavor of $\mathbb{E}[F]$ by noting that it is upper bounded by $1/p_{st}$ (evaluated at $\mathbb{E}[I]$). This is true by means of Jensen's inequality since it can be directly shown using (22) that $\mathbb{E}[F]$ is strictly concave in terms of I. The value of $\mathbb{E}[F]$ has been computed for a range of $\mathbb{E}[I]$ and results are reported in Table 2. The table clearly shows that with only $B_L = 5$ blocks, there is ample

Table 2 Average number of frames required until triangulation succeeds. A total of $B_L = 5$ resource blocks are assumed to be allocated in the random access area

$\mathbb{E}[I]$	Situation	$\mathbb{E}[F]$
3	Node closer to the network perimeter and/or heavy GPS signal blockage	2.08
5	Node in the middle of the network	13.02 and/or mild GPS signal loss
7	Node close to the network sink and/or low likelihood of GPS signal loss	81.38

time for nodes to adjust their positions. For the worst case scenario of $\mathbb{E}[I] = 7$, and assuming 1-ms frames, it takes no more than 82 ms to update the position.

5 Practical Implementation Challenges

The goal of this section will be tailored toward some of the practical challenges related to the implementation of ACR/FACR. Most of these challenges mainly stem from the nontraditional wireless channel characteristics in a cooperative transmission setup. As such, this section starts off with the presentation of the channel model which is cooperative by design. It then immediately delves into PHY design challenges invoked by the cooperative channel. Remedies and solutions are highlighted as well throughout the section.

5.1 Wireless Channel Model

From a PHY perspective, ACR in principle is a technique that allows multiple nodes to transmit the same frame almost concurrently. This statement needs to be further reinforced with respect to two different timescales. Concurrency is really true only at the packet level. At the symbol-level, however, the cooperative transmitters are not perfectly aligned in time and they need not be. In other words, the channel model has to accommodate the case of asynchronous transmission case.

In most recent literature, the case of asynchronous cooperative transmission has been referred to as the cooperative time offset (CTO) [56]. Even in the case of perfect synchronization among the I cooperative transmitters (e.g., by means of having access to GPS), there will still be time offsets from the receiver perspective due to propagation delay differences. Both effects are captured in the cooperative channel model by introducing the delays $T_1^{'} \ldots T_I^{'}$ as illustrated in Fig. 8.

The channel between an arbitrary pair of nodes is represented by a generic wide-band frequency-selective multipath tap-delay line with Rayleigh-distributed tap gains [57]. On average, there are $\mathcal{M}$ such taps. Natural echoes due to multipath are grouped in intervals of duration of T seconds. Mobility speeds are with the pedestrian to slow vehicular ranges such that the fading coefficients are assumed to be quasi-static, i.e., they remain constant during a single frame.

Orthogonal frequency division multiplexing (OFDM) is employed as a measure to counteract that frequency selectivity of the cooperative channel. The duration of the OFDM symbol is assumed to be larger than $(\mathcal{M}-1)T + \max\{T_i^{'}\}_{i=1}^{I} - \min\{T_i^{'}\}_{i=1}^{I}$ ensuring that each subcarrier encounters approximately a frequency-flat fading [58]. Amending each OFDM symbol with a cyclic prefix eliminates inter-carrier interference (ICI) and restores orthogonality between subcarriers. This enables decoupled signal detection at each subcarrier.

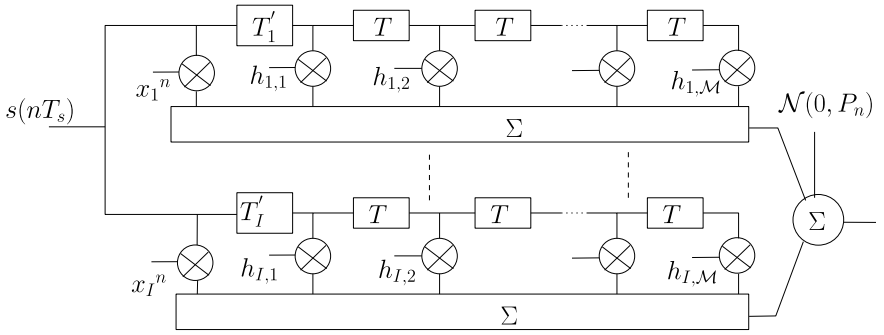

Fig. 8 Composite channel response capturing CFO plus Doppler spread, propagation delay differences, as well as multipath channel effects

Under the reasonable assumption that the fading coefficients $h_{i,m}$ are all mutually independent, it follows that $H(f)$ is complex Gaussian such that $H(f) \sim \mathcal{N}(0, \sigma_S^2)$, with

$$\sigma_S^2 = \sum_{i=1}^{I} \sum_{m=1}^{\mathcal{M}} \mathbb{E}[|h_{i,m}|^2]. \tag{23}$$

Furthermore, $|H(f)|^2$ is exponentially distributed with a mean of $2\sigma_S^2$. We note that $\sum_{m=1}^{\mathcal{M}} \mathbb{E}[|h_{i,m}|^2]$ represents the mean power content of the channel between the receiver and the ith transmitter and is equal to $(\lambda/4\pi d)^{\alpha}$. Therefore, we obtain

$$\sigma_S^2 = \left(\frac{\lambda}{4\pi}\right)^{\alpha} \sum_{i=1}^{I} \frac{1}{d_i^{\alpha}}. \tag{24}$$

It is assumed that the duration of the cyclic prefix of the OFDM symbol is long enough such that all signal echoes (natural and artificial) arrive within the cyclic prefix interval. Other ongoing packet relaying processes will rather contribute to the interference signal. This interference, however, will be also Gaussian since the individual channel gains are Gaussian [59]. The exact nature of such an external interference is beyond the scope of the present work.

5.2 Cooperative Carrier Frequency Offset

The sampling frequency is $1/T_s$, and n is a running sample index. The number of subcarriers is denoted by N_s. Due to clock imperfections, a carrier frequency offset (CFO) naturally exists between any arbitrary pair of nodes [43, 54]. The CFO between transmitter i and the receiver is denoted by $\delta_i^{(CFO)}$. The cooperative carrier frequency offset (CCFO) is defined herewith as $\max_i \delta_i^{(CFO)} - \min_i \delta_i^{(CFO)}$. On the other hand,

all nodes are assumed to be mobile; thus, a frequency Doppler exists between the ith transmitter and the receiver and is denoted by $\delta_i^{(DOP)}$. The CFO and the Doppler shift together have the combined effect of causing a phase rotation. Such an effect is captured in the model of Fig. 8 by defining:

$$x_i \triangleq e^{j2\pi\delta_i \frac{1}{N\Delta_f}} \ , \ \delta_i = \delta_i^{(CFO)} + \delta_i^{(DOP)}. \tag{25}$$

Hence, taking the individual CFO and Doppler shift effects into consideration, the baseband signal transmitted by node i is expressed as

$$\begin{aligned} s_i(nT_s) &= \sum_{k=-\frac{N_s}{2}}^{\frac{N_s}{2}} a_{k,n} e^{j\phi_{k,n}} e^{j2\pi(k\Delta f+\delta_i)nT_s} \\ &= x_i^n \sum_{k=-\frac{N_s}{2}}^{\frac{N_s}{2}} a_{k,n} e^{j\phi_{k,n}} e^{j2\pi kn/N_s}, \end{aligned} \tag{26}$$

where $a_{k,n}e^{j\phi_{k,n}}$ is the transmitted symbol. Consequently, the frequency-domain response of the composite channel is given by

$$H(n,f) = \sum_{i=1}^{I} {x_i}^n e^{-j2\pi f T_i^{'}} \sum_{m=1}^{\mathcal{M}} h_{i,m} e^{-j2\pi f(m-1)T}. \tag{27}$$

From (27), it is clear that the channel is highly time-varying because of the CCFO. This is true even though the fading coefficients are assumed to be quasi-static.

The time-varying nature of the channel mandates robust receiver design. As a matter of fact, the detrimental effect of the CCFO is far more adverse than that of the Doppler spread alone. This is true since the CCFO can be orders of magnitude larger. This is better appreciated by means of an example. A 1-ppm free-running clock yields a CFO around ± 2400 Hz at a center frequency of 2.4 GHz. In comparison, the maximum Doppler shift for a node moving at 10 km/hr, for example, is less than 25 Hz. Consequently, it is evident that the CCFO problem is order of magnitude more challenging than the classical Doppler spread problem.

In the presence of CCFO, the channel coherence time (roughly equal to the 0.423 times the reciprocal of the maximum Doppler shift [57]) in case of free-running clocks is comparable to the duration of just few OFDM symbols. The CCFO poses a couple of serious challenges on receiver design which has to cater for such a highly dynamic and fast-changing condition. Two of such challenges along with viable remedies are outlined in the following.

5.2.1 Automatic Gain Control Aging

The purpose of automatic gain control (AGC) in the receiver is to perform preamplifier gain adjustments. These adjustments are required in order for the signal to be received within the dynamic range of the analog-to-digital converter (ADC) [60]. The AGC module typically operates on the preamble portion in the very beginning of the PHY frame. It is in essence a feedback control loop whose goal is to maximize the input signal within the linear range of the ADC.

The correlation coefficient between two time samples of the Rayleigh fading envelope separated by τ_v is given by the zeroth-order first kind Bessel function $J_o(2\pi\delta_i\tau_v)$ [57]. For illustration purposes, the correlation coefficient for the case of zero CCFO (i.e., in the presence of only Doppler shifts) is compared to a 500-Hz CCFO on the same timescale in Fig. 9.

From Fig. 9, it is apparent that the AGC gain value will quickly become outdated in the presence of CCFO. This is also referred to as AGC aging. By the end of the frame, the outdated AGC value will be either:

(1) Too high, therefore driving the incoming signal to the nonlinear range of the ADC and causing significant signal distortion.
(2) Unnecessarily too low, thus the received signal may suffer from a severe SNR drop.

To address the AGC aging problem, there is the obvious option of using shorter PHY frame durations. Nevertheless, this will indeed increase the PHY overhead ratio and hence adversely affect the throughput. A more preferable option is to rerun the

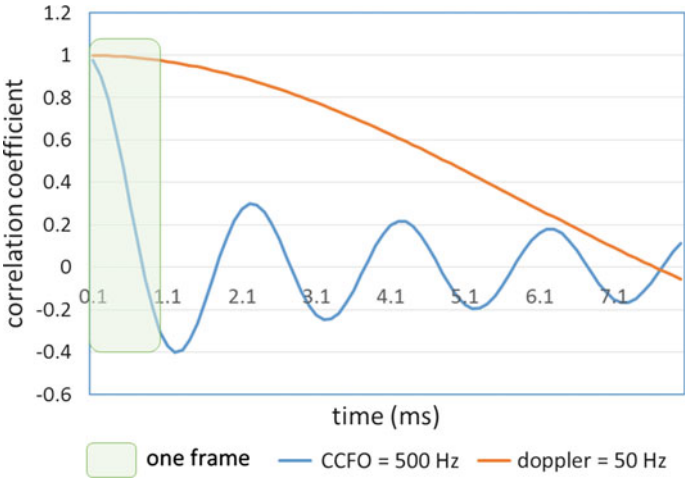

Fig. 9 Correlation coefficient of the fading channel envelope in case of zero and 500-Hz CCFO. In both cases, the Doppler shift is assumed to be 50 Hz. It is evident that CCFO produces a highly time-varying channel, and consequently, the channel gains quickly become uncorrelated even within the timescale of a single PHY frame

AGC module on pilots tones which are inserted within the PHY frame. The AGC loop may take quite a few samples in the beginning of the frame to converge. This is true since the channel variation from frame to frame may be unpredictably high. A new frame is a new transmission with a new set of cooperative transmitters. Hence, the power of the incoming signal is uncorrelated to that of the previous frame. On the other hand, the convergence time of the AGC loop when run on pilots is much faster. This is true since the channel variation within a frame is statistically correlated.

5.2.2 Aging of Channel Estimates

Similar to the AGC, channel estimation is typically performed on the preamble portion as well. Specifically, the preamble includes a long training sequence (LTS) symbol that is known a priori to the receiver. In OFDM systems, the LTS is used to estimate the fading channel coefficients corresponding to each frequency subcarrier [56]. Due to the highly time-varying nature of the channel, the estimates of the fading coefficients obtained in the beginning of the frame quickly become obsolete. In the presence of CCFO, the coherence time of the channel can be much shorter than the frame duration. As such, channel estimates need to be updated more often.

One approach is to insert more training symbols (i.e., LTS symbols) within the payload portion of the PHY frame. However, this will significantly increase the PHY overhead. This is true particularly since the coherence time is too small. For example, if the CCFO is 1000 Hz, then the coherence time of the channel is about 425 μs. A good design practice is to ensure up-to-date channel coefficients at least at a rate of 10 times per coherence window, i.e., an LTS symbol must be inserted once every 42.5 μs. For a symbol duration of 8 μs, this means that an LTS must be inserted at least after every 5th symbol. Hence, the overhead contribution of channel estimation is in excess of 16% which is quite significant.

In an attempt to relax such an overhead, one may argue for farther spacing LTS symbols in the time domain. Such a proposition would entail the use of linear interpolation to compute the amplitude and phase of the channel coefficients for OFDM symbols in between the LTS symbols. However, as Fig. 10 strongly suggests, the level crossing nature of the cooperative channel is quite aggressive thus rendering the linear interpolation option very risky.

A neater approach, on the other hand, is to autonomously estimate the channel in a continuous fashion using the well-known decision-directed estimation (DDE) method [61]. Each OFDM symbol consists of N_s samples. At the end of the LTS (which is the first symbol in the frame), the least squares (LS) channel estimate at subcarrier k is given by

$$\widehat{H}(1,k) = \frac{\sum_{n=1}^{N_s} s^*(N_s - n, k) r(N_s - n, k)}{\sum_{n=1}^{N_s} |s(N_s - n, k)|^2}, \tag{28}$$

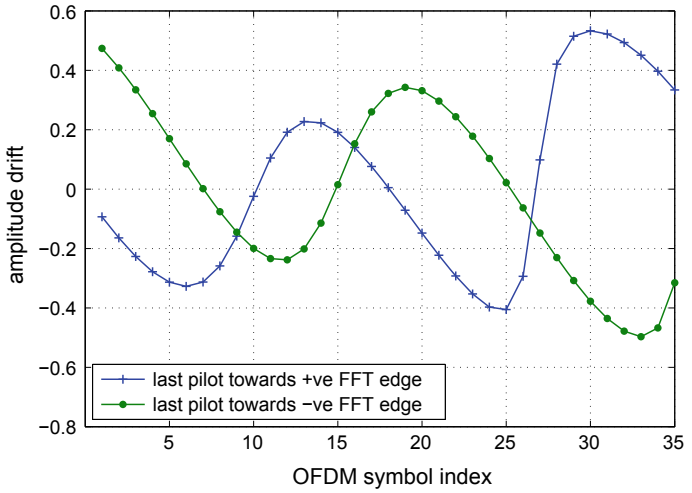

(a) Amplitude drift over time.

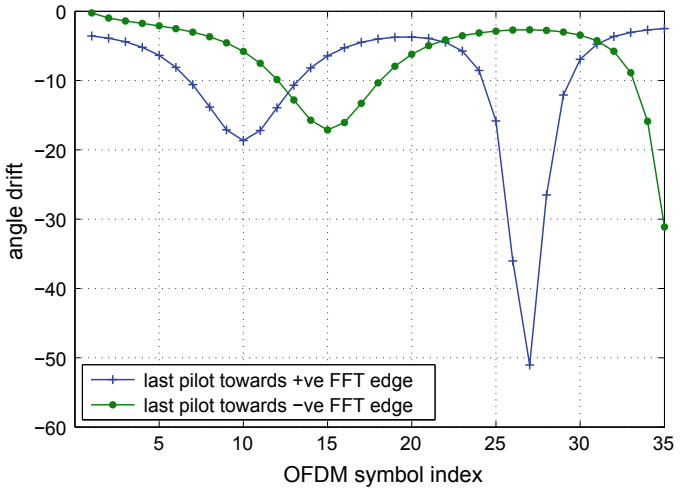

(b) Phase drift over time.

Fig. 10 Cooperative transmission in the presence of CCFO induces significant fluctuations in the phase and amplitude of channel fading coefficients. Thus, linear interpolation is by large infeasible

where $r(n, k)$ is the received signal observed at the nth time sample at the kth sub-carrier of the fast Fourier transform (FFT) stage output. In (28), $s(n, k) = p(n, k)$ when k is pilot tone, otherwise $s(n, k) = \hat{s}(n, k)$, i.e., the decided symbol. To obtain the channel estimate at any other arbitrary symbol $z = 2, 3, \ldots$, recursive estimation can used as follows:

$$\hat{H}(z,k) = \frac{\hat{y}(zN_s,k)}{\hat{Y}(zN_s,k)}, \tag{29}$$

where

$$\hat{y}(z+1,k) = \hat{y}(z,k) + r(z,k)s^*(z,k) - r(z-1,k)s^*(z-1,k) \tag{30}$$

$$\hat{Y}(z+1,k) = \hat{Y}(z,k) + |s(z,k)|^2 - |s(z-1,k)|^2. \tag{31}$$

A DDE receiver was incorporated into the PHY implementation which is further discussed in Sect. 6. Empirical results reported therewith offer clear evidence that using DDE is quite viable in treating the channel estimate aging effect.

Finally, it is worthwhile to mention that the consistent availability of a global positioning system (GPS) signal would indeed help synchronize cooperative transmitters and thus eliminate the CCFO problem. However, it is important also to emphasize that losing the GPS signal for just a few seconds may cause transmitters' clocks to drift substantially, and therefore, the CCFO problem reemerges again. This is why it is paramount to fortify receivers with GPS-independent algorithms.

5.3 Cooperative Power Delay Profile

The power delay profile (PDP) of the cooperative channel is unique in the sense that it contains many strong yet slightly delayed signal arrivals [54]. This creates a power spectral density (PSD) shape that is also fundamentally different from that corresponding to the classical PTP channel. This is illustrated in Fig. 11. As a consequence, the PDP of the cooperative channel brings forward two PHY design challenges as explained in what follows.

5.3.1 Large Dynamic Range

Channel simulations have been carried out to characterize the dynamic range of the PSD of the cooperative channel. Results are depicted in Fig. 12 where the cumulative density function (CDF) of the PSD dynamic range is plotted for two cases, $I = 1$ and $I = 3$.

The dynamic range of the channel's spectral response dictates the dynamic range of the receiver's FFT block. This is because OFDM receivers typically employ the frequency-domain equalizers (FDE) to address the frequency selectivity of the channel. The FFT block must be able to cope with larger channel dynamic ranges. Otherwise, it will cause severe degradations in the FDE performance due to clipping, and consequently, it will adversely affect the overall receiver performance. In

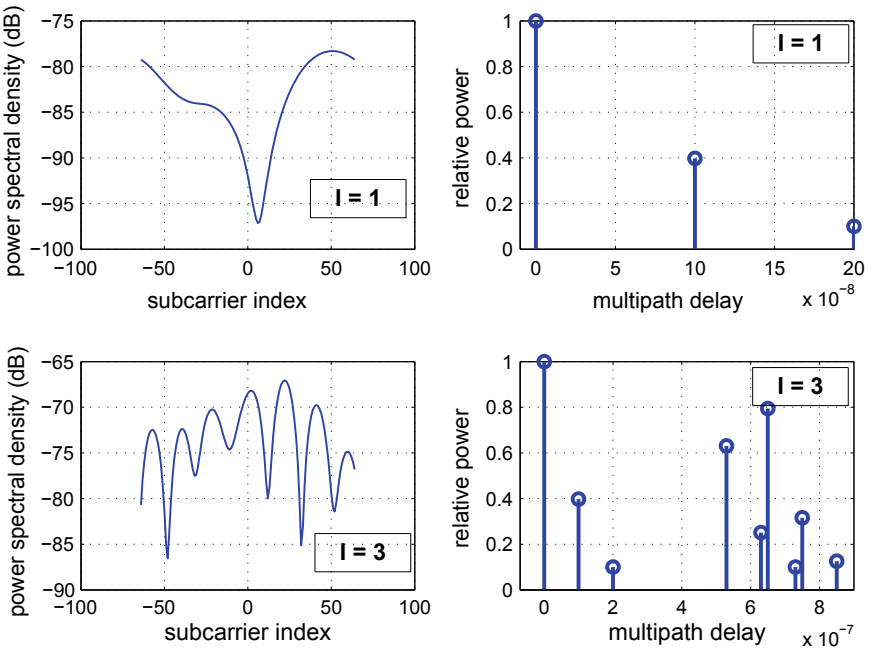

Fig. 11 The PDP and PSD of the cooperative channel (with $I = 3$) compared to that of the PTP channel. The PSD is measured over a 10 MHz channel with 128-point FFT

conclusion, the fixed-point design of the FFT block must accommodate the dynamic range requirements of cooperative transmission particularly in terms of memory resources allocated.

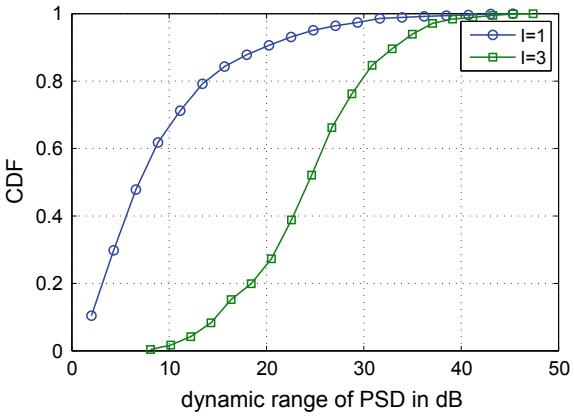

Fig. 12 The CDF of the dynamic range of the PSD. The mean dynamic range was computed to be 10.1 dB in case of one transmitter (PTP case) and 25.3 dB in case of three cooperative transmitters

5.3.2 High Frequency Selectivity

Indeed, best design practice calls for inserting pilots within the PHY frame. These pilots can be used to track phase and amplitude drifts of the channel coefficients. Pilot tones carry training symbols that are known a priori by the receiver in order to update the channel estimates. OFDM systems typically employ a comb-type pilot subcarrier arrangement whereby pilots are inserted regularly in the frequency domain [62].

Linear interpolation is mostly used to estimate channel coefficients at subcarriers between pilots. However, the frequency-domain response of the cooperative channel is quite likely not to be linear between pilots. This is further illustrated in Fig. 13. Accordingly, it is paramount to revert to nonlinear interpolation. In the implementation presented in this chapter, a three-point quadratic interpolation is carried out in accordance with [63].

Lastly, it is worthy of noting that a modern robust forward error correction (FEC) scheme is poised to address many of the challenges associated with cooperative transmission. Low-density parity-check (LDPC) codes are great candidates for this purpose [56]. The same argument applies to the use of Turbo decoders. However, it is also important to note that the remedies outlined in this section are far less demanding in terms of onboard resource utilization compared to LDPC or Turbo codes. In one instance of implementation on field programmable gate array (FPGA) platform, the inclusion of a Turbo decoder increases the resource utilization by nearly

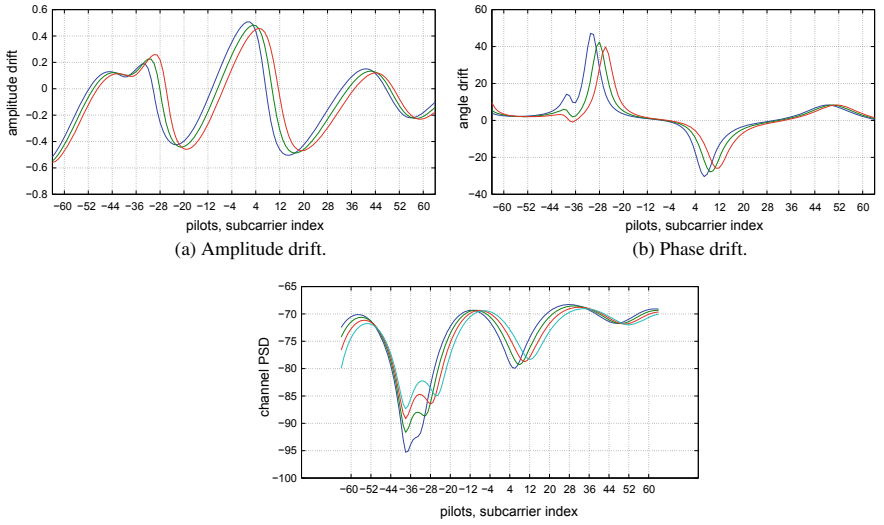

(a) Amplitude drift.

(b) Phase drift.

(c) Power spectral density.

Fig. 13 Frequency-domain response of the cooperative channel measured at pilot tones over consecutive OFDM symbols. The subcarrier indices shown in the plots correspond to the pilots. There are eight pilots allocated within the 128-point FFT

40% compared to less than 10% for the suite of DDE, AGC update, and quadratic interpolation.

5.4 Self-localization Random Access Blocks

At the receiver, the preamble portion of the OFDM frame consists of identical replicas arriving asynchronously from I nodes. As shown in Fig. 7, the receiver aligns its time reference to the first energy arrival of the first OFDM symbol. The receiver locks to the first energy arrival of the LTS symbol, which happens to be that of the second relay in this example. The picture is fundamentally different in the RA portion where each non-empty block contains a unique signal (assuming no collisions).

RA signals are generally expected to be nonaligned in time, as illustrated in Fig. 7. Time misalignments of the RA blocks obviously occur due to the differences in propagations delays between the relays toward the receiver in concern. Hence, for some RA blocks, the FFT processing window at the receiver will not be aligned in time to the actual start of the RA signal within that block.

The effect of time offsets in OFDM systems was studied in [64]. Here, the time offset is "toward" the guard interval, i.e., the FFT window is partially applied on the guard interval. It was shown in [64] that such an offset only introduces a phase error. For this reason, OOK was chosen as a modulation scheme for convenience since it is indifferent to phase rotations. Reverting to OOK for the RA entails nearly negligible increase in the FPGA resource utilization footprint. On the other hand, the use of OOK modulation is surely associated with a 3 dB SNR penalty compared to using binary phase shift keying (BPSK), for example. Nevertheless, there is an inherent power boost on RA blocks. This is because all of the transmit RF power is focused on the RA block of choice at each transmitter. This indeed helps compensate for the SNR penalty.

On the other hand, it has already been mentioned that the reconstruction of the localization waveforms is done sequentially. Such an approach is affordable since the time budget of the localization process is not quite constrained. In other words, it is acceptable for a node to take a few seconds to adjust its position information. Therefore, dedicated FPGA resources need not be allocated for localization. Instead, available resources can be exploited opportunistically. In fact, the relaxed time constraint allows to solve the hyperbolic equations associated with the triangulation function in a more powerful microcontroller processing unit (MCU), as suggested in Fig. 6.

Finally, it is worthwhile to have a peak under the hood on how the RA can be practically implemented. For a 128-point FFT, B_Q is set at 128 tones divided equally and contiguously over two consecutive symbols. Setting and $b = 6$, and allocating 64 tones per localization block yields $B_L = 5$ blocks. For 100-symbol OFDM frames, this an overhead contribution of just 6%. If the localization capability is switched off (i.e., in case of low likelihood of GPS signal loss), the overhead goes down to less than 1%. This is tangibly better than the 14–28% incurred by ACR predecessors.

According to (20), 64 quantization tones are good enough to serve $N = 95$ nodes with an average of $I = 3$ cooperative transmitters. At the other end, each OOK-modulated localization block has 128 tones or equivalently bits. With a rate $\frac{1}{2}$ FEC, this leaves 64 bits out of which 4 can be used for parity. It can be straightforwardly shown that the remaining 60 bits are sufficient to represent the GPS position offset of a node from the sink.

On the other hand, the localization resolution is actually function of the sampling rate and the number of subcarriers in each localization block. At 40 Msps, and noting that the number of samples per block is half of that of the whole OFDM symbol, then the resolution that can be achieved is 30 m. A high-performance ADC capable of higher sampling rates is indeed slightly more expensive but—if needed—can be used to achieve better resolution.

6 Experimental Performance Evaluation Results

The main goal of the field experimentation is to validate the key building block of ACR/FACR. This is to verify that multiple transmitters induce an array gain when concurrently transmitting the same packet.

6.1 Development Platform

Off-the-shelf OFDM-based transceivers (e.g., standard-based IEEE 802.11a/g or IEEE 802.16d/e) cannot be used for experimenting with cooperative transmission schemes [56]. This is due to the fact that cooperation invokes substantial changes to the PHY and lower MAC layers. Moreover, the challenges described in Sect. 5 mandate a more robust PHY design. Hence, it was decided to build the ACR/FACR protocol stack completely from scratch so as to have a sufficient level of flexibility and control over the design process.

To that end, a compact stand-alone software-defined radio (SDR) platform was selected (Fig. 14). A complete 128-point OFDM PHY was developed entirely for this project. The PHY supports channel bandwidths from 1 to 20 MHz with ADC sampling rates up to 40 Msps. The cyclic prefix consists of 32 samples such that the total number of samples per symbol is 160. The chosen SDR is home for a 40-KLE Altera Cyclone IV FPGA, an ARM9 microcontroller architecture, and a reconfigurable radio frequency (RF) chip from Lime Microsystems. An RF amplifier from Texas Instruments was also annexed to the platform. The OFDM PHY was built on the FPGA, while the rest of the protocol stack runs on the MCU.

The original plan was to install the SDR platforms on highly mobile stations to test PHY performance. However, it was shown in Sect. 5.2 that the CCFO effect produces a channel that is much more dynamic and time-varying than that produced

Fig. 14 An SDR platform from Nuand was used to build the fully autonomous cooperative routing scheme. The platform houses a 40-KLE Altera Cyclone IV FPGA, a Cypress microcontroller unit (MCU), and a reconfigurable RF chipset from Lime Microsystems. An RF amplifier from Texas Instruments was also annexed to the platform. The OFDM PHY was built on the FPGA, while the rest of the protocol stack runs on the MCU

by Doppler spread, even at high speeds. A corollary to this is that empirical results collected from the field under CCFO with *stationary* nodes are sufficient to ensure the implementation will successfully handle mobility. The key parameters concerning the underlying PHY design are reported in Table 3.

Table 3 Key OFDM PHY design parameters

Channel bandwidth	1–20 MHz
Frequency spectrum	0.3–3.8 GHz
Maximum RF transmit power	10 dBm
Antenna gain	3 dBi
FFT size	128 points
Maximum sampling rate	40 Msps
Preamble length (STS+LTS)	768 samples
Number of pilots	8
Turnaround time	180 μs
Useful symbol length	128 samples
Cyclic prefix length	32 samples

6.2 Equalizer Performance

The performance of the DDE implementation was investigated under a controlled setup. A dedicated BladeRF board was configured to feed three other boards with two common signals: clock and trigger, as shown in Fig. 15. The latter is used to instruct the three relays to commence the transmission of a frame that is prestored on the FPGA. The CFO is invoked locally at each transmitting node via a command line interface (CLI) utility. Similarly, each node may be configured to introduce a fixed delay after the rising edge of the trigger signal. This can be used to produce the

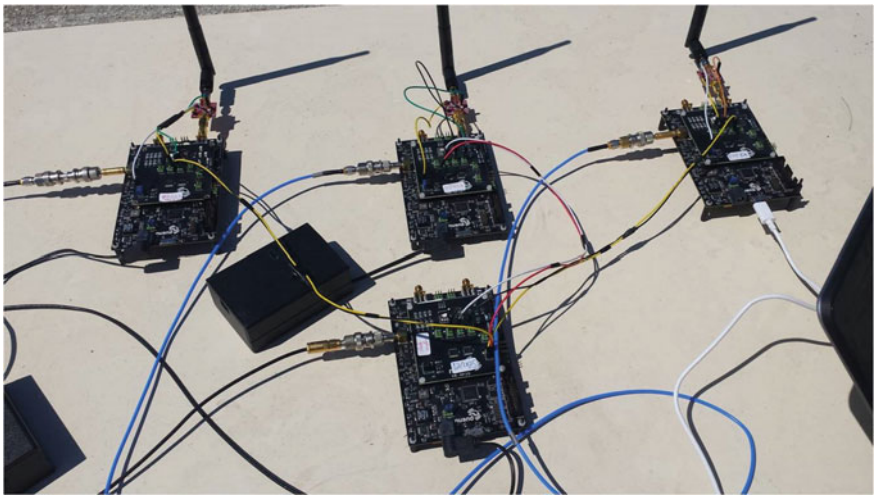

Fig. 15 Common clock and trigger signals are fed into the boards. The controlled test setup is used to measure the performance of the decision-directed equalization method

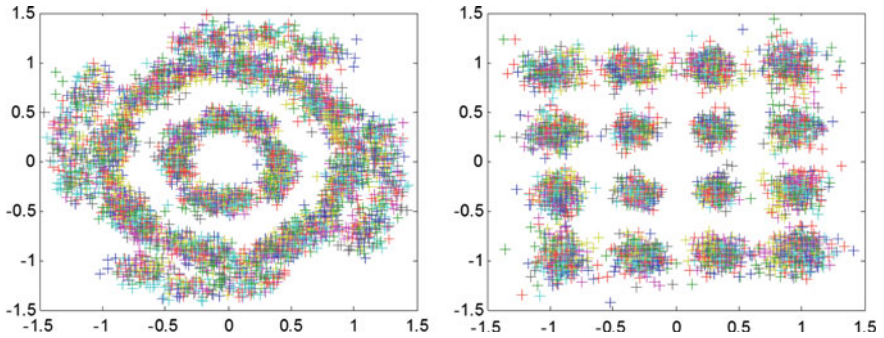

Fig. 16 DDE performance investigated for the case of concurrent transmission from three nodes with CFO1 = 1000 Hz, CFO2 = 0 Hz, CFO3 = −100Hz. Here, the received I/Q symbols are plotted

Table 4 DDE performance results

	Traditional equalizer	Decision-driven equalizer (DDE)
FER	81%	5%
EVM	−6 dB	14 dB
Highest modulation	BPSK	16 QAM

desired delay spread for the composite channel. In other words, it helps control the propagation delays $T_1^{'}, \ldots, T_I^{'}$ shown in Fig. 8.

In this test, the three transmitters were placed 12 m from the receiver. The CFO values for the transmitters were set at −100, 500, and 1000 Hz. A 16 quadrature amplitude modulation (16-QAM) modulation scheme with FEC rate of 1/2 was used. As expected, DDE is quite a viable tool to equalize highly time-varying channels. Run over a large number of iterations, the average frame error rate (FER) plunged from 81% down to less than 5% when the DDE module was activated at the receiver. The error vector magnitude (EVM) of the baseband inphase/quadrature (I/Q) stream was measured on randomly selected subset of frames in MATLAB (Fig. 16). The average EVM ascended from as low as −6 to 14 dB. Neglecting transmitter I/Q imperfections, the EVM is known to be tightly related to the receiver SNR. As such, the DDE module can be said to offer a gain of nearly 20 dB while introducing less than 5% in the overall footprint of the PHY code. These results are summarized in Table 4.

Table 5 Results from the array gain test

	SNR (dB)	RSSI (dBm)	FER (%)	reach (m)
Tx_1 only	16.1	−88.2	2.9	70
	11.2	−93.1	50.8	115
Tx_2 only	16.5	−87.5	0.8	65
	11.8	−94.1	76.2	115
Tx_3 only	16.4	−88.0	1.1	65
	12.4	−93.5	47.0	115
All three	16.3	−86.7	2.0	115

6.3 Array Gain

The goal of this test case was to measure the array gain as well as the maximum reach gain that can be obtained by means of autonomous cooperative transmission. The same setup presented in the previous subsection was used. To obtain the maximum reach gain, the CFO was forced to zero on all three transmitters. The three transmitters were always kept equidistant from the receiver. The test was carried out in an open space parking lot surrounded by light vegetation. All nodes were placed one meter above ground level. Results of this test are reported in Table 5. Each result corresponds to an average value taken over an ensemble of 10,000 frames.

The first stage of this stage was to measure the communication range for each individual transmitter. The communication range here was defined as the maximum reach such that an average FER target of $\leq 3\%$ is maintained. The receiver was gradually moved away in steps of 5 m. As reported in Table 5, the communication range was around 65–70 m. The slight discrepancy in results is due to the different multipath channels since transmitters are not co-located. Another factor is the approximate nature of any method for computing the SNR on the preamble signal.

Next, the communication range for the case of three cooperative transmitters was measured by gradually moving the receiver away in steps of 5 m. The maximum range was measured to be 115 m, i.e., the reach gain was 50 m or equivalently 77%. Indeed, the reach gain highly depends on the propagation characteristics, which in return relates to the environment where the test is performed.

Now in order to characterize the array gain, each transmitter was placed 115 m away from the receiver and the SNR was measured. The array gain is computed here as the difference between the SNR obtained under cooperative transmission and the average of individual SNR values. It is clear from Table 5 that autonomous cooperative transmission is able to offer nearly 4.5 dB of array gain. This result is quite interesting since it is very close to the theoretical maximum array gain with three transmitters, i.e., $10 \log 3 = 4.77$ dB.

7 Conclusions

There is a growing trend for streaming live vision-based data from the field to enhance visibility and assist decision-making during mission-critical situations. The dissemination of live vision-based data feeds demands high bandwidth in addition to low latency.

Over-the-counter wireless technologies available today have been shown to fall short in meeting the demands of next-generation mission-critical applications. As such, mobile ad hoc networking (MANET) has resurfaced again as a viable contender in place of Wi-Fi and LTE. Having said that, classical path-oriented MANET routing techniques are notoriously known to accumulate substantial protocol overhead as the network grows in scale. Subsequently, it has been shown that autonomous cooperative routing (ACR) is well positioned to meet the goals and requirements of mission-critical operations.

To that end, the implementation of ACR on commercial hardware platforms entails a few practical challenges which have not been quite addressed in literature. The foremost challenge concerns the receiver's capability in handling the aggressive nature of the cooperative wireless channel. The cooperative channel is highly time-varying therefore causing channel estimates to become obsolete pretty quickly. A robust channel equalizer based on the use of decision-drive estimation (DDE) was presented to remedy this issue. On the other hand, the cooperative channel has been shown to feature a high level of selectivity in the spectral domain which was handled by means of optimized pilot signal processing. The chapter also presented a fully astomous version of ACR. Practical implementation considerations have been also highlighted offering some evidence of the advents of full autonomy.

Finally, the chapter presented an experimental setup that was developed specifically to validate the basic building blocks of ACR/FACR. A protocol stack was built from scratch for that purpose. Field experiments were carried out and were able to validate some of the performance enhancement propositions outlined in the various sections of the chapter.

References

1. Suriyachai, P., Roedig, U., Scott, A.: A survey of mac protocols for mission-critical applications in wireless sensor networks. IEEE Commun. Surv. Tutor. **14**(2), 240–264 (2012)
2. Fink, J., Ribeiro, A., Kumar, V.: Robust control of mobility and communications in autonomous robot teams. IEEE Access **1**, 290–309 (2013)
3. Ghafoor, S., Sutton, P.D., Sreenan, C.J., Brown, K.N.: Cognitive radio for disaster response networks: survey, potential, and challenges. IEEE Wirel. Commun. **21**(5), 70–80 (2014)
4. Akyildiz, I., Melodia, T., Chowdhury, K.: A survey on wireless multimedia sensor networks. Elsevier J. Comput. Netw. **51**(4), 921–960 (2007)
5. Zhang, Z.J., Lai, C.F., Chao, H.C.: A green data transmission mechanism for wireless multimedia sensor networks using information fusion. IEEE Wirel. Commun. **21**(4), 14–19 (2014)
6. Yang, L., Yang, S.-H., Plotnick, L.: How the Internet of Things technology enhances emergency response operations. Technol. Forecast. Soc. Change Elsevier **80**(9), 1854–1867 (2013)

7. Chai, P.R.: Wearable devices and biosensing: Future frontiers. J. Med. Toxicol. 1–3 (2016)
8. Panayides, A., Antoniou, Z.C., Mylonas, Y., Pattichis, M.S., Pitsillides, A., Pattichis, C.S.: High-resolution, low-delay, and error-resilient medical ultrasound video communication using h.264/avc over mobile wimax networks. IEEE J. Biomed. Health. Inform. **17**(3), 619–628 (2013)
9. Bergstrand, F., Landgren, J.: Using live video for information sharing in emergency response work. Int. J. Emerg. Manag. **6**(3–4), 295–301 (2009)
10. Blair, A., Brown, T., Chugg, K.M., Halford, T.R., Johnson, M.: Barrage relay networks for cooperative transport in tactical manets. In MILCOM 2008—2008 IEEE Military Communications Conference, Nov 2008, pp. 1–7
11. Bergstrand, F., Landgren, J.: Visual reporting in time-critical work: exploring video use in emergency response. In: Proceedings of the 13th International Conference on Human Computer Interaction with Mobile Devices and Services, pp. 415–424 (2011)
12. Nunes, D.S., Zhang, P., Sa Silva, J.: A survey on human-in-the-loop applications towards an internet of all. IEEE Commun. Surv. Tutor. **17**(2), 944–965 (2015)
13. Felts, R., Leh, M., McElvaney, T.: Public safety analytics r&d roadmap. National Institute of Standards and Technology (NIST), U.S. Department of Commerce, Technical Note 1917, Apr 2016
14. Bayezit, I., Fidan, B.: Distributed cohesive motion control of flight vehicle formations. IEEE Trans. Ind. Electron. **60**(12), 5763–5772 (2013)
15. Berni, J., Zarco-Tejada, P.J., Suarez, L., Fereres, E.: Thermal and narrowband multispectral remote sensing for vegetation monitoring from an unmanned aerial vehicle. IEEE Trans. Geosci. Remote Sens. **47**(3), 722–738 (2009)
16. Siebert, S., Teizer, J.: Mobile 3d mapping for surveying earthwork projects using an unmanned aerial vehicle (uav) system. Autom. Constr. Elsevier **41**, 1–14 (2014)
17. Lin, X., Andrews, J.G., Ghosh, A., Ratasuk, R.: An overview of 3g pp device-to-device proximity services. IEEE Commun. Mag. **52**(4), 40–48 (2014)
18. Bader, A., Ghazzai, H., Kadri, A., Alouini, M.S.: Front-end intelligence for large-scale application-oriented internet-of-things. IEEE Access **4**, 3257–3272 (2016)
19. Carl, L., Fantacci, R., Gei, F., Marabissi, D., Micciullo, L.: Lte enhancements for public safety and security communications to support group multimedia communications. IEEE Netw. **30**(1), 80–85 (2016)
20. Gharbieh, M., ElSawy, H., Bader, A., Alouini, M.-S.: Tractable stochastic geometry model for iot access in lte networks. In: To Appear in Proceedings of IEEE Globecom 2016, Washington D.C., December 2016
21. Kiess, W., Mauve, M.: A survey on real-world implementations of mobile ad-hoc networks. Ad Hoc Netw. **5**(3), 324–339 (2007)
22. Bellalta, B.: IEEE 802.11ax: high-efficiency wlans. IEEE Wirel. Commun. **23**(1), 38–46 (2016)
23. Abouzeid, A.A., Bisnik, N.: Geographic protocol information and capacity deficit in mobile wireless ad hoc networks. IEEE Trans. Inf. Theory **57**(8), 5133–5150 (2011)
24. Request for information, novel methods for information sharing in large scale mobile ad-hoc networks, defense advanced research projects agency (darpa), darpa-sn-13-35, April 2013
25. Halford, T.R., Chugg, K.M., Polydoros, A.: Barrage relay networks: system and protocol design. In: 21st Annual IEEE International Symposium on Personal, pp. 1133–1138. Sept, Indoor and Mobile Radio Communications (2010)
26. Halford, T.R., Chugg, K.M.: Barrage relay networks. In: Information Theory and Applications Workshop (ITA), 2010, Jan 2010, pp. 1–8
27. Acer, U.G., Kalyanaraman, S., Abouzeid, A.A.: Weak state routing for large-scale dynamic networks. IEEE/ACM Trans. Netw. **18**(5), 1450–1463 (2010)
28. Halford, T.R., Chugg, K.M.: The stability of multihop transport with autonomous cooperation. In: 2011—MILCOM 2011 Military Communications Conference, Nov 2011, pp. 1023–1028
29. Bader, A., Abed-Meraim, K., Alouini, M.-S.: An efficient multi-carrier position-based packet forwarding protocol for wireless sensor networks. IEEE Trans. Wirel. Commun. **11**(1), 305–315 (2012)

30. Lakshmi, V., Thanayankizil, A.K., Ingram, M.A.: Opportunistic large array concentric routing algorithm (olacra) for upstream routing in wireless sensor networks. Ad Hoc Netw. **9**(7), 1140–1153 (2011)
31. Ke, C.-K., Chen, Y.-L., Chang, Y.-C., Zeng, Y.-L.: Opportunistic large array concentric routing algorithms with relay nodes for wireless sensor networks. Comput. Electr, Eng (2016)
32. Halford, T.R., Courtade, T.A., Turck, K.A.: The user capacity of barrage relay networks. In: MILCOM 2012—2012 IEEE Military Communications Conference, Oct 2012, pp. 1–6
33. Xiang, X., Wang, X., Zhou, Z.: Self-adaptive on-demand geographic routing for mobile ad hoc networks. IEEE Trans. Mob. Comput. **11**(9), 1572–1586 (2012)
34. Intelligent transport systems (its); vehicular communications; geonetworking; part 4: geographical addressing and forwarding for point-to-point and point-to-multipoint communications; sub-part 1: Media-independent functionality, v1.2.0, Oct 2013
35. Sanchez, J., Ruiz, P., Marin-Perez, R.: Beacon-less geographic routing made practical: challenges, design guidelines, and protocols. IEEE Commmun. Mag. **47**(8), 85–91 (2009)
36. Scaglione, A., Goeckel, D., Laneman, J.: Cooperative communications in mobile ad hoc networks. IEEE Signal Process. Mag. **23**(5), 18–29 (2006)
37. Sirkeci-Mergen, B., Scaglione, A.: Randomized space-time coding for distributed cooperative communication. ICC (2006)
38. Sirkeci-Mergen, B., Scaglione, A.: Randomized space-time coding for distributed cooperative communication. IEEE Trans. Signal Process. **55**(10), 5003–5017 (2007)
39. Sharp, M., Scaglione, A., Sirkeci-Mergen, B.: Randomized cooperation in asynchronous dispersive links. IEEE Trans. Commun. **57**(1), 64–68 (2009)
40. Li, Y., Zhang, Z., Wang, C., Zhao, W., Chen, H.-H.: Blind cooperative communications for multihop ad hoc wireless networks. IEEE Trans. Veh. Technol. **62**(7), 3110–3122 (2013)
41. Brian, R.H., Hwang, G.: Barrage relay networks for unmanned ground systems. In: Military Communications Conference, 2010—MILCOM 2010, Oct 2010, pp. 1274–1280
42. Lee, D.K., Chugg, K.M.: A pragmatic approach to cooperative communication. In: MILCOM 2006—2006 IEEE Military Communications Conference, Oct 2006, pp. 1–7
43. Bader, A., Alouini, M.-S.: An ultra-low-latency geo-routing scheme for team-based unmanned vehicular applications. In: IEEE Globecom Workshops (GC Wkshps), 2015. IEEE, pp. 1–6 (2015)
44. Bader, A., Alouini, M.S.: Localized power control for multihop large-scale internet of things. IEEE Internet of Things J. **3**(4), 503–510 (2016)
45. Zorzi, M., Rao, R.: Geographic random forwarding (GeRaF) for ad hoc and sensor networks: multihop performance. IEEE Trans. Mob. Comput. **2**(4), 337–348 (2003)
46. Gupta, P., Kumar, P.R.: The capacity of wireless networks. IEEE Trans. Inf. Theory **46**(2), 388–404 (2000)
47. Bisnik, N., Abouzeid, A.A.: Queuing network models for delay analysis of multihop wireless ad hoc networks. Ad Hoc Netw. Elsevier **7**(1), 79–97 (2009)
48. Bisnik, N., Abouzeid, A.A.: Queuing delay and achievable throughput in random access wireless ad hoc networks. In: 2006 3rd Annual IEEE Communications Society on Sensor and Ad Hoc Communications and Networks, Sept 3, pp. 874–880 (2006)
49. Wu, H., Peng, Y., Long, K., Cheng, S., Ma, J.: Performance of reliable transport protocol over ieee 802.11 wireless lan: analysis and enhancement. In: INFOCOM 2002. Twenty-First Annual Joint Conference of the IEEE Computer and Communications Societies. Proceedings, vol. 2, pp. 599–607. IEEE (2002)
50. Bader, A., Abed-Meraim, K., Alouini, M.S.: Reduction of buffering requirements: Another advantage of cooperative transmission. IEEE Sens. J. **15**(4), 2017–2018 (2015)
51. McDonald, A.B., Znati, T.F.: A mobility-based framework for adaptive clustering in wireless ad hoc networks. IEEE J. Sel. Areas Commun. **17**(8), 1466–1487 (1999)
52. Squartini, T., Picciolo, F., Ruzzenenti, F., Garlaschelli, D.: Reciprocity of weighted networks. Scientific reports, vol. 3, 2013
53. Eriksson, M., Mahmud, A.: Dynamic single frequency networks in wireless multihop networks—energy aware routing algorithms with performance analysis. In: Proceedings of

The 10th IEEE International Conference on Computer and Information Technology, Bradford, UK, pp. 400–406, May 2010
54. Bader, A., Alouini, M.S.: Mobile ad hoc networks in bandwidth-demanding mission-critical applications: practical implementation insights. IEEE Access **5**, 891–910 (2017)
55. Srinivasa, S., Haenggi, M.: Distance distributions in finite uniformly random networks: theory and applications. IEEE Trans. Veh. Technol. **59**(2), 940–949 (2010)
56. Qiu, H., Wang, K., Psounis, K., Caire, G., Chugg, K.M.: High-rate wifi broadcasting in crowded scenarios via lightweight coordination of multiple access points. In: MobiHoc '16 Proceedings of the 17th ACM International Symposium on Mobile Ad Hoc Networking and Computing, July 2016, pp. 301–310
57. Rappaport, T.: Wireless Communications: Priciples and Practice, 2nd edn. Prentice Hall (2001)
58. Schulze, H., Lueders, C.: Theory and Applications of OFDM and CDMA, 1st edn. John Wiley and Sons Ltd (2005)
59. Zhao, B., Valenti, M.C.: Practical relay networks: a generalization of hybrid-ARQ. IEEE J. Sel. Areas Commun. **23**(1) (2005)
60. Rouphael, T.J.: Wireless Receiver Architectures and Design: Antennas, RF. Mixed Signal, and Digital Signal Processing. Elsevier, Synthesizers (2014)
61. Ran, J., Grunheid, R., Rohling, H., Bolinth, E., Kern, R.: Decision-directed channel estimation method for OFDM systems with high velocities. In: Vehicular Technology Conference, 2003. VTC 2003-Spring. The 57th IEEE Semiannual, April 2003, vol. 4, pp. 2358–2361
62. Hsieh, M.-H., Wei, C.-H.: Channel estimation for OFDM systems based on comb-type pilot arrangement in frequency selective fading channels. IEEE Trans. Consum. Electron. **44**(1), 217–225 (1998)
63. Coleri, S., Ergen, M., Puri, A., Bahai, A.: Channel estimation techniques based on pilot arrangement in ofdm systems. IEEE Trans. Broadcast. **48**(3), 223–229 (2002)
64. Athaudage, C.: BER sensitivity of OFDM systems to time synchronization error. In: The 8th International Conference on Communication Systems (ICCS'02), Singapore, vol. 1, pp. 42–46, Nov 2002